8016927

FELDT, ANDREW NEIL

NON-LTE EFFECTS IN SUPERNOVA ENVELOPES

The University of Oklahoma PH.D. 1980

University Microfilms International 300 N. Zeeb Road, Ann Arbor, MI 48106 18 Bedford Row, London WC1R 4EJ, England

THE UNIVERSITY OF OKLAHOMA

GRADUATE COLLEGE

NON-LTE EFFECTS IN SUPERNOVA ENVELOPES

A DISSERTATION

SUBMITTED TO THE GRADUATE FACULTY

in partial fulfillment of the requirements for the

degree of

DOCTOR OF PHILOSOPHY

BY

ANDREW NEIL FELDT

Norman, Oklahoma

1980

NON-LTE EFFECTS IN SUPERNOVA ENVELOPES

APPROVED BY

DISSERTATION COMMITTEE

ACKNOWLEDGEMENTS

I am grateful to Dr. David Branch for all his guidance and especially for helping me to learn how to think about complicated problems in terms of simple physics. I also appreciate his patience in the interminably slow development of this thesis. I am indebted to Dr. Guido Chincarini, Dr. Roger Frech, Dr. Tibor Herczeg, and Dr. Michael Morrison for all of the helpful suggestions and corrections contributed upon their reading of this manuscript. I thank the Department of Physics and Astronomy and the University of Oklahoma for financial support and the use of the computing facilities necessary for this work. Last, and most important, I thank my wife, Jan, for countless hours of typing, retyping, correcting my inadequate English, and for all the emotional support without which this work would never have been completed.

TABLE OF CONTENTS

LIST OF TABLES

LIST OF FIGURES

LIST OF FIGURES (cont'd)

ABSTRACT

The Sobolev method has been applied to the solution of the statistical rate equations for multi-level representations of singly ionized silicon and neutral hydrogen for various models of supernova envelopes. The physical models are based on the power law models of Branch [1977]. The electron temperature in the envelope is taken as isothermal or as decreasing outward in the envelope as derived for a gray, spherical atmosphere. Radiation is treated for two cases. In the dilute case, the radiation field is simply the dilute photospheric radiation except when the continuum becomes optically thick where it is replaced by the diffuse radiation field in the approximation given by Castor and Van Blerkom [1970]. In the discontinuous opacity case, the size of the photosphere is allowed to extend indefinitely for frequencies greater than some transition frequency. Thus, some lines and continua are treated in the dilute case while others see only the local radiation. In all cases the resulting source functions and line optical depths are compared to those obtained by less detailed calculations with good agreement.

NON-LTE EFFECTS IN SUPERNOVA ENVELOPES

CHAPTER I

INTRODUCTION

Supernovae have been recognized as a distinct class of celestial objects since Baade and Zwicky proposed the name in 1934 [Baade and Zwicky, 1934]. They are stellar objects which, like novae, suddenly become very bright and then fade over a period of time. However, by the study of both types in nearby galaxies [Zwicky, 1965], it is clear that supernovae are over one thousand times brighter than novae. The brightest novae may achieve a luminosity one million times brighter than that of the sun, so supernovae are over one billion times brighter than the sun. The luminosities of whole galaxies range from 10^6 to 10^{11} solar luminosities. Thus, a single supernova may rival or exceed its parent galaxy in brightness.

The study of supernovae is hampered by their relative infrequency. In our own galaxy there has been an average of one per 250 years visible from earth based on records over roughly the past 2000 years [Clark and Stephenson, 1976], the last being observed by Kepler in 1604. Presently, somewhat over 20 supernovae are discovered each year in other galaxies. It is from these supernovae that observations are drawn which provide clues to their nature.

The observational quantities of supernovae which we have to work with are their light curves (the time variation of the luminosities), the variation of their colors with time and their spectra. From these, it has been found that supernovae can be divided into two types, Type I and Type II [Minkowski, 1941], although other types have been suggested to explain peculiar supernovae [Zwicky, 1965].

Type I supernovae are characterized by the following: a) The light curves are all very similar. Following maximum light (the time of peak luminosity) there is a rapid drop in luminosity for about 20 days. This is followed by a more gentle, exponential decay in luminosity. An average Type I light curve, following Barbon et. al. [1973], is shown in Figure 1a. b) The colors are blue at maximum light, suggesting a temperature of over 10,000 K, and redden with increasing time. c) The spectra show strong, broad features near maximum light, but the presence of hydrogen is questionable at best.

For Type II supernovae, the following characteristics apply: a) The light curves vary greatly from one supernova to the next, but they do not resemble those of Type I. A "normal" Type II light curve, following Barbon et. al. [1979], is, nonetheless, shown in Figure 1b. The "shoulder" in the light curve is usually present although its duration and slope can vary greatly. Type II supernovae appear to be roughly three times fainter than Type I at maximum light [Branch and Bettis, 1978]. b) The colors vary like those of Type I, but are bluer at maxi-

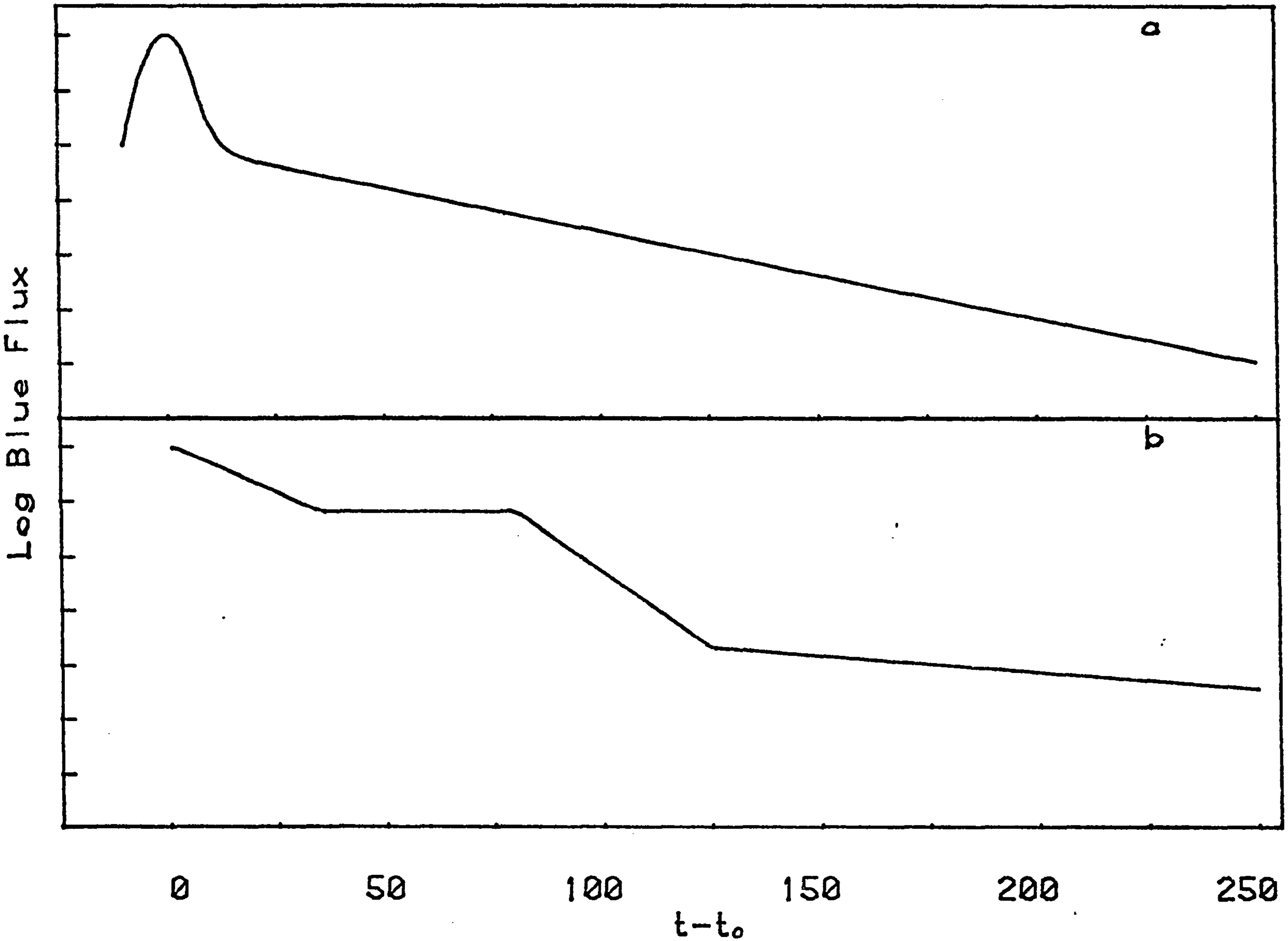

Figure 1. Supernova Light Curves.

mum light, suggesting a larger temperature. c) The spectra are nearly featureless at maximum light. As time progresses, the Balmer lines become strong and other lines appear.

The bulk of our understanding of individual stars comes from the interpretation of their spectra. Spectra of supernovae were taken as early as 1895 [Johnson, 1936]. However, these spectra have only recently become interpretable. In part, this is due to acceptance of a thermal model for the envelopes around supernovae near maximum light. The essence of this model is that the continuum radiation is produced by a rapidly expanding, cooling photosphere [Arp, 1961; Pskovskii, 1969]. The lines are produced by scattering in the differentially expanding atmosphere above the photosphere, yielding typical P-Cygni profiles. These profiles have an emission part about the rest wavelength of the line and an absorption part blueshifted by roughly the velocity of the envelope where the line is formed. This can be understood by looking at surfaces of constant line-of-sight velocity in the expanding envelope. In cylindrical coordinates (z, p, ϕ) with the z-axis along the line of sight, the line-of-sight velocity at some point, $R = (z^2 + p^2)^{\frac{1}{2}}$, in the envelope is given by

$$V_z = V(R)\frac{z}{R} \qquad \text{Eq. 1}$$

But for $V(R) \propto R$, as expected after an explosion,

$$V_z \propto z \qquad \text{Eq. 2}$$

Therefore, the surfaces of constant velocity are planes perpendicular to the z-axis. This is illustrated in Figure 2 showing the relationship between these surfaces and a typical profile. For reasons to be ex-

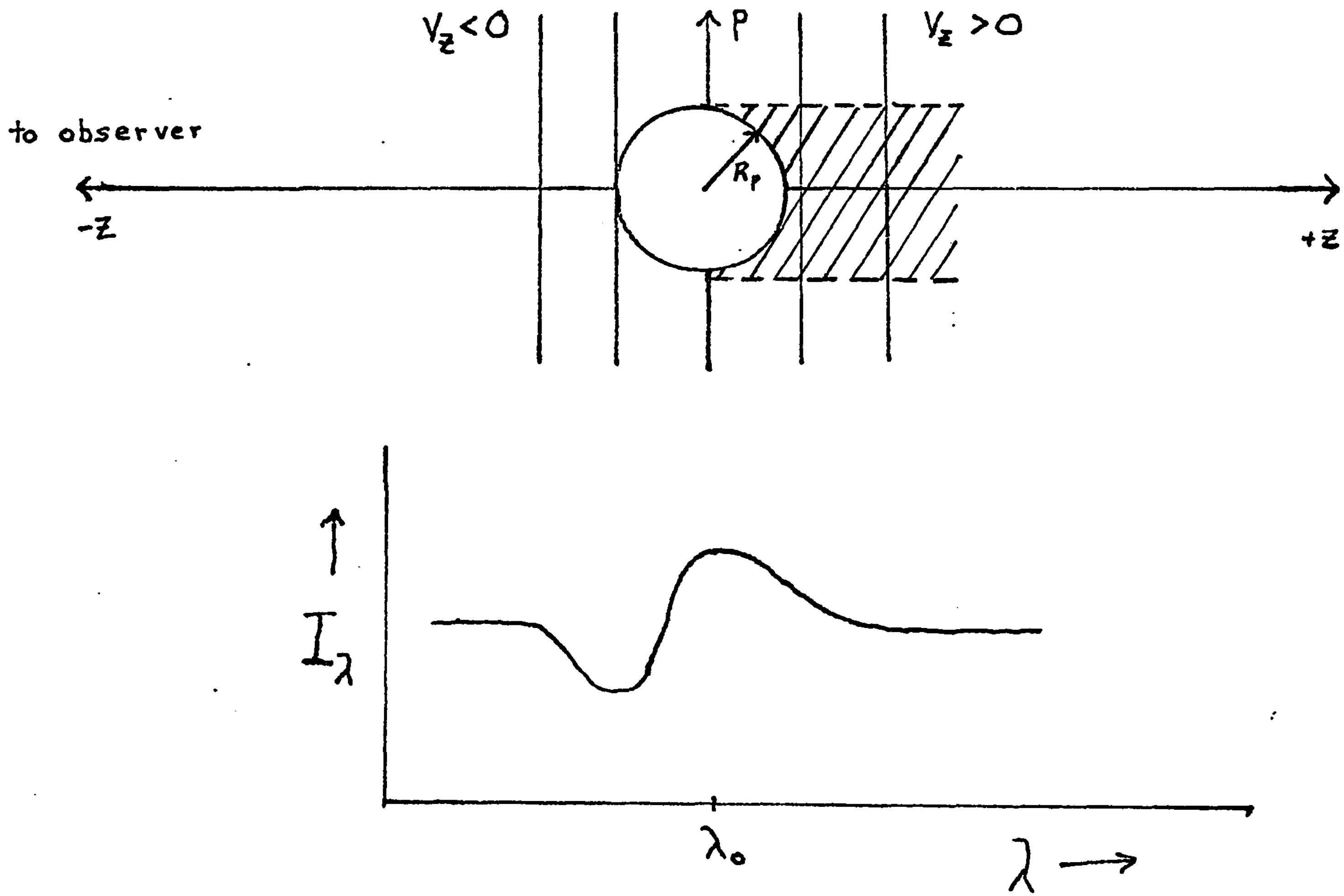

Figure 2. Surfaces of Constant Velocity and P-Cygni Profile.

plained later, lines can be expected to form quite near the photosphere. Thus, identifying a line having an absorption component gives a measure of the velocity of the material at the photosphere, V_p. The identification of the Si II λ6355 line in Type I supernovae has indicated $V_p \approx$ 11,000 km/s [Branch, 1977], while hydrogen lines in Type II supernovae have indicated $V_p \approx$ 7,000 km/s [Patchett and Branch, 1972].

The radius of the photosphere, R_p, as a function of time can be investigated by the method first suggested by Baade [1926] for variable stars. In its simplest form, the ratio of the radius at one time to that at another is found from the Stefan-Boltzmann law, where, for a blackbody of radius R and a temperature T, the luminosity is given by

$$L = 4\pi R^2 \sigma T^4 \qquad \text{Eq. 3}$$

so that

$$R_1/R_2 = (L_1/L_2)^{\frac{1}{2}}(T_2/T_1)^2 \qquad \text{Eq. 4}$$

where subscripts refer to the values at two different times. If the velocity as a function of time is known, the difference in radius, R_2-R_1, can be found by integrating the velocity over time. Thus, the actual radii and, from Equation 3, the actual luminosity may be found. Since we are dealing with a single object at a fixed distance, the ratio of the intrinsic luminosities is given by the ratio of the observed luminosities.. The (blackbody) temperature can be derived from the colors. In practice, luminosities are only observed in certain frequency bands, but the basic principle still applies. In a fashion like this, Branch [1977, 1979] has shown that R_p increases linearly with time for Type I up to about 20 days past maximum light, while this is roughly true for Type II supernovae up to about 1-1/2 months past maximum light. The photosphere is fixed in the material for Type I while for Type II supernovae the photosphere slowly falls back with respect to the medium [Kirshner and Kwan, 1974].

Support for these conclusions comes from studies of supernova hydrodynamics. A good review of this topic has been written by Chevalier [1980]. It is found that if $\sim 10^{50}$ to 10^{52} ergs are deposited at the center of a massive star, a shock wave is propagated outward which leaves behind a differentially expanding envelope with velocity proportional to radius, each mass element coasting at a constant velocity [Lasher, 1975; Chevalier, 1976; Falk and Arnett, 1977; Weaver and Woosley, 1978].

The next step in the process of understanding supernovae is the quantitative analysis of their spectra. This is important for several reasons. First, supernovae are expected to be a primary site for the expulsion of the products of nucleosynthesis. Thus, the chemical composition of supernova envelopes is important for understanding the solar abundances of elements and the chemical evolution of galaxies [Tinsley, 1977b].

Supernovae are also an important tool in cosmology. If the intrinsic luminosity of a supernova can be determined, the apparent luminosity then gives the distance which, with the redshift of the parent galaxy, can be used to determine H_0, the expansion rate of the universe. This has been done for individual supernovae [Kirshner and Kwan, 1974; Schurmann et. al., 1979] and for composite light curves and colors [Branch and Patchett, 1973; Branch, 1977, 1979]. Since supernovae are so bright, they may be able to probe far enough into the universe to measure q_0, the deceleration parameter, as suggested by Wagoner [1977], for example. However, the radii and temperatures used to determine the luminosity by the Baade method are derived from the spectra and colors and thus are susceptible to assumptions about the spectra.

Given the physical conditions expected in the envelope (Chapter II), local thermodynamic equilibrium (LTE) conditions are not to be expected, so that line intensities may not be calculated in the usual fashion. Instead, the statistical rate equations must be solved to find the level populations at each point in the envelope. Normally, this involves the simultaneous solution for the transfer of line radiation and therefore a large scale iterative procedure. However, because of the rapid differential expansion of the envelope, line transfer may be treated as developed by Sobolev [1960] and Castor [1970]. Photons generated at a point are either reabsorbed locally or are Doppler-shifted out of resonance and then either strike the photosphere or escape completely. This allows the radiation field to be treated in a local fashion.

There have been many attempts at line identification in supernovae near maximum light based on LTE populations or comparison with novae. For a good review of this topic, see Oke and Searle [1974]. More recent papers have built on the earlier views [Mustel', 1975; Patchett and Wood, 1976; Kirshner et. al., 1976; Assousa et. al. 1976; Ciatti and Rosino, 1977a, 1977b]. Some non-LTE calculations using the Sobolev method have been presented by Kirshner and Kwan [1974] and Gordon [1975] for one month past maximum light. However, the understanding of certain lines is crucial in understanding supernovae. The identification of the λ6355 line of Si II has been used to determine the photospheric velocity of Type I. The line appears to be unblended and is strong throughout the period near maximum light. It is important to know whether this identification can be verified with a reasonable physical model of the envelope. If so, the line profile will be useful for exploring the structure of the envelope. When lines begin to appear in Type II supernovae, the Balmer lines are dominant, while they are apparently completely missing in Type I. It is important to place limits on the amount of hydrogen in Type I supernovae so that realistic hydrodynamic models can be constructed [Lasher et.al., 1977]. Also, the search for likely progenitors is constrained by the envelope composition [Tinsley, 1977a].

The purpose of this paper is to explore the deviations from LTE of the level populations of Si II in Type I supernovae and hydrogen in Type II in the context of various physical models discussed in Chapter II. Any understanding of hydrogen in Type II will easily be transferred to Type I supernovae. The treatment of the radiation field will follow the Sobolev method as presented in Chapter III. The models all consider only the time near maximum light during the linear (or near linear) expansion of the photosphere. All models also follow the development of the envelope as a function of time and consider several radius points. Priority is given to the atomic levels which control the strength of the observed lines. As discussed in Chapter IV, the atoms are represented by enough levels so the high priority level populations should be well determined. The final chapter presents the results and discussion.

CHAPTER II

PHYSICAL MODELS OF THE ENVELOPE

Several models of the envelope were considered, but all were centered on a basic model formulated by Branch [1977] derived from composite light curves and colors. He assumed the temperature, T, and density, ρ, in the envelope varied as powers of radius, R, and time, t, as

$$T \propto R^{-p} t^{p-s} \qquad \text{Eq. 5}$$

$$\rho \propto R^{-n} t^{n-3} \qquad \text{Eq. 6}$$

and that the opacity, k, varied as powers of T and ρ as

$$k \propto T^{m} \rho^{q} \qquad \text{Eq. 7}$$

and showed that this implied

$$R_p \propto t^{x} \qquad \text{Eq. 8}$$

where

$$x = \frac{m(p-s) + (q+1)(n-3)}{mp + n(q+1) - 1} \qquad \text{Eq. 9}$$

Since x is known to be near unity from the near linear variation of the photospheric radius with time and the lack of change of Doppler shifts in unblended lines during the phases of interest, a reasonable set of the parameters which satisfy this are necessary. The simplest way to accomplish this is via a strong density gradient, i.e. if n is large $x \simeq 1$. If the opacity is independent of T and ρ ($m = q = 0$), then

$$x = \frac{n - 3}{n - 1} \qquad \text{Eq. 10}$$

Hydrodynamic calculations [Colgate and McKee, 1969] have related the velocity in the envelope to the external mass fraction, F, so that

$$V(R) \propto F(R)^{-1/4} \qquad \text{Eq. 11}$$

If $V(R) \propto R$ and Equation 6 is assumed, then since

$$F(R) \propto \int_R^\infty \rho(r) r^2 dr \qquad \text{Eq. 12}$$

Equation 11 becomes

$$R \propto R^{(n-3)/4} \qquad \text{Eq. 13}$$

so that n = 7. Calculations by Weaver [private communication] based on hydrodynamic modeling also show agreement with $\rho \propto r^{-7}$. Therefore, this density structure was adopted for all calculations.

The total density at the photosphere at maximum light is determined by assuming $N_e \propto R^{-7}$ and requiring that the electron scattering optical depth, τ_e, be equal to three for thermalization. The optical depth is given by $\tau(R) = \int_R^\infty N(r)\sigma(r)dr$ where σ is the absorption cross-section. It is roughly equivalent to the number of photon mean free paths from the point R to the observer. The requirement that τ_e be equal to three at the photosphere is due to estimates of the relative contribution of lines to the opacity [Karp et. al., 1977] which forms the photosphere. The assumption that $N_e \propto R^{-7}$ will be examined in Chapter V. The density is then taken to follow Equation 6 with n = 7. Mass elements traveling at constant velocity decrease in density as t^{-3} due to expansion.

Electron densities were then calculated by the algorithm given by Karp [1980] which ensures swift convergence. The thirteen most abundant elements [Ross and Aller, 1976] were used for this purpose. These and

TABLE I

Elemental Abundances

Element	Log N
H	12.00
He	10.80
C	8.62
N	7.94
O	8.84
Ne	7.57
Na	6.28
Mg	7.60
Al	6.52
Si	7.65
Ca	6.35
Fe	7.50
Ni	6.28

their abundances (normalized to log $N_H = 12$, where N_H is the number density of hydrogen) are listed in Table I.

Since Type I supernovae are likely to be deficient in hydrogen [Bychkova and Bychkov, 1977] and their actual composition is unknown, three compositions were considered: solar abundance, no hydrogen and no hydrogen or helium. Type II models were assumed to have solar abundances.

The photosphere is assumed to radiate like a blackbody. This is consistent with the derivation of the temperatures from the colors. The photospheric temperatures and radii as a function of time and the photospheric velocities at maximum light come from Branch [private communication]. Table II lists these for Type II supernovae and compares them with the results of selected hydrodynamic models. The agreement is quite good. Table III simply lists the adopted temperatures and radii for Type I supernovae for which there are not such detailed comparisons available. The photospheric velocity is taken to be 10,000 km/s at all times. Lasher [1975] has shown that the light curve and colors of Type I supernovae can be reproduced by a hydrodynamic model similar to those referred to in Table II.

The electron temperature in the envelope is taken to be isothermal and equal to the temperature of the photosphere or is assumed to be given by the expression Van Blerkom [1973] has derived for a gray, spherically symmetric atmosphere in radiative equilibrium. For $\rho \propto r^{-7}$ his formula gives

$$T(r) = T(R_p) r^{-0.6} \left(\frac{21}{26} r^{-6} + \frac{5}{26}\right)^{1/4} \qquad \text{Eq. 14}$$

where $r = R/R_p$. With the preceeding as a base, the following two types

TABLE II

Physical Parameters of Type II Supernovae

$t-t_o$	T_p (10^3 K)				R_p (10^{15} cm)				V_p (10^3 km/s)			
(days)	CH	FA	WW	Present	CH	FA	WW	Present	CH	FA	WW	Present
0	14.	42.	40.	25.	.74	.10	.10	.39	8.8	7.1	12.	7.0
3	12.	18.	16.	17.	.97	.30	.33	.57	8.3	7.9	6.9	7.0
7	10.	13.	11.	12.	1.2	.58	.67	.83	7.8	8.0	6.5	7.0
15	8.3	8.5	7.5	8.7	1.6	1.1	1.3	1.3	7.1	7.9	6.3	6.9
30	6.3	6.1	6.2	6.2	2.0	1.8	2.1	1.8	5.8	5.5	5.2	5.8
45	---	---	5.8	5.3	---	---	2.3	2.8	---	---	4.2	6.4

TABLE III

Physical Parameters of Type I Supernovae

$t-t_o$ (days)	T_p (10^3 K)	R_p (10^{15} cm)
-5	35.	.55
0	17.	1.0
5	12.	1.5
10	9.3	1.9
15	7.7	2.4
20	6.2	2.8
25	4.9	3.3

of models are considered.

Dilute Models

The photosphere is assumed to be well-defined, producing a dilute, blackbody radiation field in the surrounding envelope. The mean continuum intensity, J_ν, was treated following Castor and Van Blerkom [1970] so that core and diffuse components were considered. Thus,

$$J_\nu = J_\nu^c + J_\nu^d \qquad \text{Eq. 15}$$

where

$$J_\nu^c = WB_\nu(T_p)\exp(-\tau_c) \qquad \text{Eq. 16}$$

is the dilute core radiation decreased according to the continuum optical depth, τ_c, which is found by trapezoidal integration. W is the geometrical dilution factor given by

$$W = \tfrac{1}{2}(1 - (1 - r^{-2})^{\frac{1}{2}}) \qquad \text{Eq. 17}$$

This is simply $1/4\pi$ times the solid angle subtended by the photosphere from the point r. Even though the envelope is not homogeneous, the diffuse component was taken to be

$$J_\nu^d = S_\nu[1 - \exp(-\tau_c)] \qquad \text{Eq. 18}$$

where the continuum source function is given by

$$S_\nu = \frac{2h\nu^3}{c^2}(b_i\exp(h\nu/kT_e) - 1)^{-1} \qquad \text{Eq. 19}$$

This was only done to keep the equations in a local form.

In the calculations of the electron densities, the ionization ratios are assumed to deviate from their LTE values (at the temperature of the photosphere) by the factor $W^2(T_e/T_p)^{\frac{1}{2}}$, assuming photoionization from excited levels dominates. This factor will be discussed and explained in Chapter V. When considering hydrogen, the actual deviation coefficient is used for its contribution to the electron density.

Discontinuous Opacity Model

It is well known that Type I supernovae are flux deficient below 4000 Å [Holm et.al., 1974 ; Zwicky, 1965]. One possible explanation is an increase in opacity with decreasing wavelength. This will increase the photospheric size with decreasing wavelength since a greater opacity at some frequency means that one does not have to look as deeply into the atmosphere before it becomes opaque. For some point in the envelope, high frequency radiation will then be at the local blackbody intensity while lower frequency radiation will be dilute from a deeper photosphere. Because of this, the ionizing radiation may be Planckian at a lower temperature (if a temperature gradient is considered) than deduced from observations of light in the visible and infrared.
As a first approximation, one might assume that all populations are driven to their LTE values. In this paper, a cutoff frequency was considered such that the photosphere was indefinitely large for $\nu > \nu_c$ The continuum radiation was taken to be only the diffuse component with τ_c set to infinity for $\nu > \nu_c$. The radiation was considered in the dilute fashion for $\nu < \nu_c$. In the calculations of N_e, the ionization ratios are assumed to be at their LTE values for the local electron temperature with the exception of hydrogen as noted for the dilute case. This model is an extreme which should place limits on the effects of a more realistic change in opacity.

CHAPTER III

METHOD

In statistical equilibrium, which is assumed, the level populations of an ion are determined by the fact that the rate of transition into any level is equal to the rate out of that level. So, we write for level i,

$$\sum_{j\neq i} N_j(C_{ji} + R_{ji}) + N_e{}^2 N^+ \gamma_i + N_e N^+ \alpha_i$$
$$= N_i\{\sum_{j\neq i}(C_{ij} + R_{ij}) + C_{i\kappa} + R_{i\kappa}\} \qquad \text{Eq. 20}$$

where N_i is the number density of the i^{th} level of the ion, N^+ is the number density of the next ionization stage, C_{ij} and R_{ij} are the collisional and radiative bound-bound rates from level i to level j, γ_i and α_i are the collisional and radiative recombination coefficients, and $C_{i\kappa}$ and $R_{i\kappa}$ are the collisional and radiative ionization rates. The R_{ij} depend on the mean intensity of the radiation field in the transition, $\langle J_{ij}\rangle$. (For a downward transition, $R_{ij} = A_{ij} + B_{ij}\langle J_{ij}\rangle$ where A_{ij} and B_{ij} are the Einstein coefficients for spontaneous and stimulated emission.) This field is normally non-local, depending on the level populations at all points in a static stellar atmosphere.

In an expanding envelope the situation can be simplified. Sobolev [1960] first introduced the concept of the escape probability in the treatment of radiative transfer in moving media. He defined the escape probability, β, as the "fraction of the quanta in the corresponding line (which) will leave the medium owing to the Doppler effect." Instead of a balance of transitions, there is an excess of downward transitions from level i to level j given by $N_i A_{ij} \beta_{ij}$. Neglecting collisional and stimulated transitions, these excess rates must be balanced by ionization and recombination so that Equation 20 becomes

$$\sum_{j>i} N_j A_{ji} \beta_{ij} + N_e N^+ \alpha_i = N_i \left(\sum_{j=1}^{i-1} A_{ij} \beta_{ji} + R_{i\kappa} \right) \qquad \text{Eq. 21}$$

Sobolev derived a crude expression for the escape probability by assuming a homogenous, infinite, expanding medium and considering a photon traveling from one point to another distant one in a spectral line with a rectangular profile. The fraction of radiation absorbed (which must equal 1 - β) is then found by integrating the absorption coefficient times the line profile function over the line element. This gave an expression for the escape probability in terms of the velocity gradient and level populations

$$\beta_{\ell u} = \left\{ \frac{\pi e^2}{mc} g_\ell f_{\ell u} (N_\ell / g_\ell - N_u / g_u) \right\}^{-1} \frac{\nu_{u\ell}}{c} \frac{dV(s)}{ds} \qquad \text{Eq. 22}$$

where ℓ and u refer to the lower and upper levels of the transition g is the statistical weight, f is the oscillator strength, ν is the transition frequency and $\frac{dV(s)}{ds}$ is the velocity gradient along the line element. The important idea here is that a large velocity gradient produces a large escape probability due to the fact that the photon is more rapidly Doppler-shifted out of resonance. However, this expression for the escape "probability" can become larger than unity for very small level populations or large velocity gradients.

Castor [1970] has further developed the Sobolev method by considering the complete radiation field (due to the line and from the continuum) and by only assuming the natural line profile is very narrow. This yields a more satisfactory form for the escape probability,

$$\beta_{\ell u} = \beta_{u\ell} = \int_0^1 \frac{1 + \sigma x^2}{\tau_{\ell u}} \{1 - \exp[-\tau_{\ell u}/(1 + \sigma x^2)]\} dx \qquad \text{Eq. 23}$$

where

$$\sigma = \frac{d\ln V(R)}{d\ln R} - 1 \qquad \text{Eq. 24}$$

and the line optical depth is given by

$$\tau_{\ell u} = \frac{\pi e^2}{mc} g_\ell f_{\ell u} (N_\ell/g_\ell - N_u/g_u)/(\frac{\nu_{u\ell}}{c} \frac{V(R)}{R}) F(\sigma) \qquad \text{Eq. 25}$$

where $F(\sigma)$ is of order unity. For a linear relation between V and R, $\sigma = 0$ and $F(\sigma) = 1$ so that

$$\beta_{\ell u} = (1 - \exp\{-\tau_{\ell u}\})/\tau_{\ell u} \qquad \text{Eq. 26}$$

This reduces to Sobolev's expression when τ is large (and β is small) and approaches unity for vanishing line optical depth.

Now the radiation field in the line can be written in terms of the line source function, $S_{u\ell}$, and the photospheric radiation intensity, I_p, as

$$\langle J_{u\ell}\rangle = (1 - \beta_{u\ell})S_{u\ell} + \beta_{u\ell} W I_p \qquad \text{Eq. 27}$$

where

$$S_{u\ell} = N_u A_{u\ell}/(N_\ell B_{\ell u} - N_u B_{u\ell}) \qquad \text{Eq. 28}$$

This allows the radiation field in a line which is optically thick to be dominated by the local line source function and that for an optically thin line to be dominated by the dilute photospheric radiation.

Thus, $\langle J_{u\ell}\rangle$ is written in terms of local parameters. The complete equation for level i becomes

$$\sum_{u>i} N_u (N_e c_{ui} + A_{ui}\beta_{ui} + B_{ui}\beta_{ui} W I_p)$$
$$+ \sum_{\ell<i} N_\ell (N_e c_{\ell i} + B_{\ell i}\beta_{\ell i} W I_p) + N_e N^+ (N_e \gamma_i + \alpha_i)$$
$$= N_i \{ \sum_{u>i} (N_e c_{iu} + B_{iu}\beta_{iu} W I_p) + \sum_{\ell<i} (N_e c_{i\ell} + A_{i\ell}\beta_{i\ell} + B_{i\ell}\beta_{i\ell} W I_p)$$
$$+ N_e c_{i\kappa} + 4\pi \int_{\nu_i}^{\infty} a_i(\nu) \frac{J_\nu}{h\nu} [1 - \exp(-h\nu/kT_e)/b_i] d\nu \} \qquad \text{Eq. 29}$$

where $c_{ui} = C_{ui}/N_e$, $a_i(\nu)$ is the photoionization cross-section of the i^{th} level, J_ν is the mean intensity of the continuum radiation field, T_e is the local electron temperature and b_i is the coefficient of deviation from LTE, $b_i = N_i/N_i^*$, where N_i^* is the Boltzmann population for the current N_e and N^+ [Mihalas, 1978].

Castor and Van Blerkom [1970], Castor and Nussbaumer [1972], and Oegerle and Van Blerkom [1976a] have solved the statistical rate equations in this form for He II, C III, and He I in Wolf-Rayet envelopes. These stars are ejecting matter at the relatively slow speed of ∿2000 km/s. Oegerle and Van Blerkom [1976b] and Van Blerkom [1978] have also applied the method to He I and H in P-Cygni which is ejecting matter with a speed of a few tens of km/s. In all cases, the results compare quite favorably with observations of line intensities and profiles. Since we are dealing with larger velocity gradients in supernova envelopes, the Sobolev method is even more appropriate as the line photons will be more quickly Doppler-shifted out of resonance.

By Equations 25 and 26 we see that the escape probabilities depend on the (unknown) level populations in a non-linear way. This means that we must estimate the populations, calculate the escape probabilities and iterate until convergence is achieved. Convergence for non-linear problems is not a trivial matter. Others have approached the problem by requiring the fractional change in all populations to be less than some criterion [e.g. Castor and Van Blerkom, 1970; Oegerle and Van Blerkom, 1976a]. This approach was adopted here with some modifications. The primary convergence criterion was

$$|(N_i^{(k)} - N_i^{(k-1)})/N_i^{(k)}| < .01 \qquad \text{Eq. 30}$$

where k is the iteration index and i labels the atomic level. Since there is primary interest in the populations of certain levels, a slightly more global criterion was used so that

$$|(N_i^{(k)} - N_i^{(k-4)})/N_i^{(k)}| < .01 \qquad \text{Eq. 31}$$

for those levels. It was also required that the change in population for these levels be decreasing at the time of convergence, so that

$$|\Delta_i^{(k)}| < |\Delta_i^{(k-1)}| \qquad \text{Eq. 32}$$

where

$$\Delta_i^{(k)} = N_i^{(k)} - N_i^{(k-1)} \qquad \text{Eq. 33}$$

Another difficulty in non-linear problems can be slow convergence. In order to speed convergence, a modified Newton-Raphson scheme was applied to each level population. If the populations were to change quadratically as a function of iteration number, the "final" population in level i based on information obtained by iteration k would be given by

$$N_i^{(k)'} = N_i^{(k)} + \tfrac{1}{2}(\Delta_i^{(k)})^2/(\Delta_i^{(k-1)} - \Delta_i^{(k)}) \qquad \text{Eq. 34}$$

This only works if $N_i^{(k)}$ is convex with respect to iteration number and so is used only if $|\Delta_i^{(k)}| < |\Delta_i^{(k-1)}|$. If $|\Delta_i^{(k)}| \geq |\Delta_i^{(k-1)}|$, there is no general way to estimate $N_i^{(k)'}$, so the form used here was $N_i^{(k)'} = N_i^{(k)} + 10\Delta_i^{(k)}$. If $\Delta_i^{(k)}$ and $\Delta_i^{(k-1)}$ had opposite signs, $N_i^{(k)'}$

was simply set equal to $N_i^{(k)}$ to avoid pushing the population too far in one direction.

These calculations were done at five radius points for each model and time considered: at r = 1, 1.1, 1.2, 1.3 1.4. For $\rho \propto r^{-7}$, at r = 1.4 the density has decreased by a factor of ten from at the photosphere. The times relative to maximum light which were considered are those listed in Tables II and III.

CHAPTER IV

ATOMIC REPRESENTATIONS AND RATES

Representations

Since the statistical rate equations must be solved for the level populations, some finite number of levels must be chosen. One procedure is to choose enough levels so that the uppermost are nearly in LTE via collisional processes. Griem [1963] has given a formula for determining this for hydrogenic atoms. He finds that for principal quantum number $n \geq n_0$, the populations will be within 10% of their LTE value with

$$n_0 = \left\{\frac{7.4\times10^{18} z^6}{N_e}\left(\frac{kT_e}{E_H}\right)^{\frac{1}{2}}\right\}^{2/17} \qquad \text{Eq. 35}$$

where z is the nuclear charge and E_H is the ionization potential of hydrogen. In the best case (for the physical models considered; $N_e \simeq 7\times10^{10}$ cm^{-3}, T = 25,000 K), n_0 = 8. However, in the worst case ($N_e \simeq 10^5$ cm^{-3}; T ≃ 3000 K), $n_0>30$. To keep the problem tractable for consideration of several physical models, it is desirable to represent the atoms with 20 levels or less.

Another procedure is to consider which atomic levels directly affect the population of the levels of interest. For Si II, the 4s ^2S level is of primary interest since it controls the strength of the λ6355 (4s ^2S - 4p $^2P^0$) transition. Of secondary interest is the 3d ^2D level which controls the next strongest line in the visible at λ4130 (3d ^2D - 4f $^2F^0$). Radiative rates dominate collisional rates for these transitions. This can be seen by the following. The collisional rate can be approximated [Van Regemorter, 1962] by

$$N_e c = N_e 13.7 f T_e^{-\frac{1}{2}} P(E/kT_e) E^{-1} \qquad \text{Eq. 36}$$

where f is the oscillator strength, P is a tabulated function ≃0.2 for ions and E is the excitation energy in cm^{-1}. The radiative rate is given [Wiese et.al., 1969] by

$$A = .667 g_\ell f/g_u\ E^2 \qquad \text{Eq. 37}$$

where g_ℓ is the statistical weight of the lower level and g_u is the statistical weight of the upper level. So

$$\frac{N_e c}{A} \simeq 4.1 N_e T_e^{-\frac{1}{2}} g_u/g_\ell\ E^{-3} \qquad \text{Eq. 38}$$

For the λ6355 transition, E ≃ 16,000 cm^{-1}, g_u= 6, and g_ℓ = 2. Thus, for N_e = $3\text{x}10^{11}$ cm^{-3} and T = 35,000 K, this ratio is ∿$5\text{x}10^{-3}$. For the λ4130 transition, E ≃ 24,000 cm^{-1}, g_u = 14 and g_ℓ = 10, yielding a ratio of ∿$6\text{x}10^{-4}$. Since the electron density drops more rapidly (both as a function of time and radius) than the square root of the temperature this is the largest these ratios can be.

So, let us look at radiative rates into the 4s ^2S level considering transitions from the 4p, 5p, and 6p $^2P^0$ levels. We find $A_{5p,4s}/A_{4p,4s}$ ≃ $6.6\text{x}10^{-3}$ and $A_{6p,4s}/A_{4p,4s}$ ≃ $3.8\text{x}10^{-3}$. For radiative rates into the 3d ^2D level, consider transitions from 4p, 5p, 6p $^2P^0$ and 4f and 5f $^2F^0$. This gives $A_{4p,3d}/A_{4f,3d}$ ≃ $1.2\text{x}10^{-3}$, $A_{5p,3d}/A_{4f,3d}$ ≃ $1.3\text{x}10^{-2}$, $A_{6p,3d}/A_{4f,3d}$ ≃ $5.8\text{x}10^{-3}$ and $A_{5f,3d}/A_{4f,3d}$ ≃ .5. This indicates that considering energy levels up to the 6p $^2P^0$ and 5f $^2F^0$ levels should

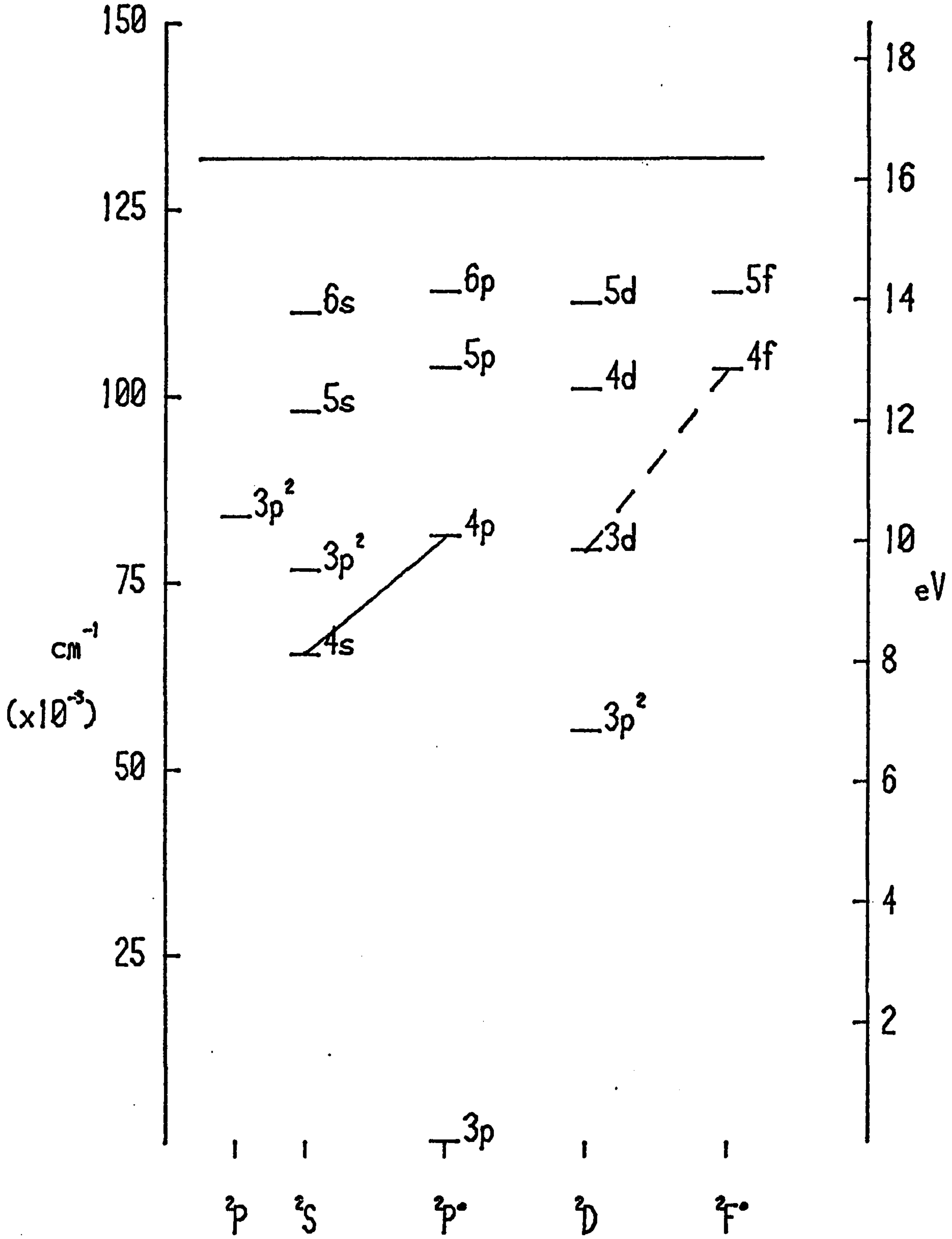

Figure 3. Representation of Si II.

include all levels affecting the population of the 4s ^2S level and may be adequate for the 3d ^2D level. Quartets (which do not interact with the doublet terms) have been ignored. The adopted representation of Si II is shown in Figure 3.

Similarly, for hydrogen where the n=2 level is of interest, radiative rates dominate and we find $A_{10,2}/A_{3,2} \approx 10^{-3}$. Therefore, by including 10 levels, all levels which directly influence the n=2 level will be included.

One other consideration is whether complete redistribution in the angular momentum sublevels can be assumed. The most serious problem would occur if the electron density were so low that 2-photon decay from the $2\ ^2S$ level would occur more rapidly than collisional transfer to the $2\ ^2P$ level. The critical density for this is $N_e \approx 10^4$ cm^{-3} [Osterbrock, 1974], which is never reached. Therefore, the hydrogen atom will be represented by the n=1 through n=10 levels.

Rates

The final information necessary for solving the rate equations involves the atomic transition rates. These can be divided into two categories: radiative rates and collisional rates.

Oscillator strengths were taken from Wiese et.al. [1969] except that, for Si II, the 3p $^2P^0$ - 3p^2 ^2D, 3p^2 ^2S, 3d ^2D, and 4d ^2D f-values were taken from Curtis and Smith [1974], the 3p $^2P^0$ - 3p^2 ^2P f-value was taken from Livingston et.al. [1976] and all f-values for allowed transitions not found elsewhere were taken from Kurucz and Peytremann [1975]. The Einstein coefficients were calculated from the oscillator strengths in the usual fashion.

Photoionization rates were determined by integration over the photoionization cross-sections as shown in Equation 7. These cross-sections were calculated as hydrogenic for both hydrogen and Si II, so that

$$a_i(\nu) = 7.9\text{x}10^{-18} g_i n_i (\nu_0/\nu)^3/z^2 \qquad \text{Eq. 39}$$

where n_i is the effective quantum number of level i, g_i is the statistical Gaunt factor, ν_i is the threshold frequency and z is the effective charge. For hydrogen, the Gaunt factors for n=1 and n=2 were taken to be 0.8 and 0.9 respectively [Allen, 1973]. For all other hydrogen levels and all Si II levels the Gaunt factor was set to unity. For hydrogen, the n_i are just the principal quantum numbers and z = 1. For Si II, z was taken to be 2 and n_i was determined by assuming the 5f $^2F^0$ level had n_i = 5 and then by scaling by ionization energy as if Si II were hydrogenic. That is, $n_i = n_{5f}(I_{5f}/I_i)^{1/2}$ where I_i is the ionization energy of level i. This provided agreement, on the average, with the cross-sections for the 3p $^2P^0$, 4s ^2S, 3d ^2D and 4p $^2P^0$ levels listed in Allen [1955]. For these four levels, the n_i were adjusted so that actual agreement was achieved.

Radiative recombination rates were determined by the Milne relation from the photoionization cross-sections

$$\alpha_i = 2/\sqrt{2\pi}\frac{h^3}{c^2}(mkT_e)^{-3/2}(g_i/g^+)\nu_0{}^3\exp(h\nu_0/kT_e)a_i(\nu_0)E_1(h\nu_0/kT_e) \qquad \text{Eq. 40}$$

where g^+ is the statistical weight of the upper ion, and $E_1(x)$ is the first exponential integral of x.

Although collisional rates were only important for the upper levels of hydrogen and a few transitions in Si II, they were calculated for all transitions.

For Si II, excitation and de-excitation rates were calculated [Van Regemorter, 1962] by

$$c_{\ell u} = 19.73 T_e^{-3/2} f_{\ell u} P(x) \exp(-x)/x \qquad \text{Eq. 41}$$

$$c_{u\ell} = c_{\ell u} \exp(x) \qquad \text{Eq. 42}$$

where $x = E/kT_e$, E is the excitation energy and P(x) is tabulated. The tabulated function was made analytic by fitting the following formulae to it.

$$\begin{aligned} P(x) &= .29 E_1(x) && x<0.01 \\ &= -.59 \log x - .026 && 0.01<x<0.2 \\ &= .167 (\log x)^2 - .126 \log x + .219 && 0.2<x<3.5 \\ &= .2 && 3.5<x \end{aligned} \qquad \text{Eq. 43}$$

For hydrogen, the formula of Johnson [1972] was used to calculate excitation and de-excitation rates. For excitation (n'>n),

$$\begin{aligned} c_{nn'} = {} & \left(\frac{8kT_e}{\pi m}\right)^{\frac{1}{2}} \frac{2n}{y} \pi a_0^2 x^2 \{\theta_{nn'} [(\frac{1}{x} + \tfrac{1}{2}) E_1(x) - (\frac{1}{z} + \tfrac{1}{2}) E_1(z)] \\ & + (\xi_{nn'} - \theta_{nn'} \ln \frac{2n^2}{y}) [\frac{1}{x} E_2(x) - \frac{1}{z} E_2(z)]\} \end{aligned} \qquad \text{Eq. 44}$$

where $x = E_{nn'}/kT_e$, $y = 1 - (\frac{n}{n'})^2$, $z = x + r_{nn'}$, $r_{1n'} = .45x$, $r_{n>1,n'} = 1.94 n^{-1.57}$, $\theta_{nn'} = \frac{2n^2}{x} f_{nn'}$, $\xi_{nn'} = \frac{4n^4}{n'^3} x^{-2} (1 + \frac{4}{3} x^{-1} + \eta_n x^{-2})$, $\eta_n = n^{-1}(4.0 - 18.63 n^{-1} + 36.24 n^{-2} - 28.09 n^{-3})$ for $n \geq 2$, $\eta_1 = -0.603$, $E_2(x)$ is the second exponential integral, and a_0 is the first Bohr radius. Again, de-excitation rates follow from Equation 42.

The collisional ionization rates for Si II were calculated by the formula of Seaton [1964]

$$c_{i\kappa} = 2.0 \times 10^{-8} \zeta I^{-2} T_e^{\frac{1}{2}} 10^{(-5040 I/T_e)} \qquad \text{Eq. 45}$$

where ζ is the number of electrons in the ionizing shell and I is the ionization energy in eV. ζ was set to unity for all levels.

For hydrogen, the collisional ionization rates were calculated by integration of the cross-sections of Percival [1966] over a Maxwellian velocity distribution.

All three-body recombinations coefficients were calculated by detailed balancing, so that they are given by

$$\gamma_i = (N_e{}^*N^{+*})^{-1}N_i{}^*c_{i\kappa} \qquad \text{Eq. 46}$$

CHAPTER V

RESULTS AND DISCUSSION

The models described in Chapter II were explored as described in Chapter III with the computations being done on the IBM 370/158 computer at the University of Oklahoma. Typical running times for a model were 15 minutes CPU for Si II and 7 minutes CPU for hydrogen.

At this point, tables of level populations could be presented, but they would have little meaning. If one wishes to construct synthetic spectra, it is not practical to solve the statistical rate equations for each ion under consideration. Rather, a more crude, but faster, method is preferred for predicting the level populations. For the discontinuous opacity models, the assumption of LTE populations might be a reasonable approximation since the ionizing radiation and radiation exciting most from the ground is the local Planckian field.

For the dilute models, a different approach can be taken. Since we are considering a radiation dominated situation, the levels which are populated directly from the ground level will be excited by the dilute photospheric radiation. Thus, the excitation of these levels should be given by

$$N_i/N_1 = \frac{WI_P(\nu)}{B_\nu}(N_i/N_1)^* \qquad \text{Eq. 47}$$

where ν is the frequency in the transition from the excited level to the ground, B_ν is the blackbody intensity at frequency ν and * refers to the LTE excitation at the photospheric temperature. In this paper, the photospheric radiation has been assumed to be blackbody, so that Equation 47 becomes

$$N_i/N_1 = W(N_i/N_1)^* \qquad \text{Eq. 48}$$

Some levels may not be excited directly from the ground. For such a level, there may exist a lower level which controls the population so that

$$N_u/N_\ell = W(N_u/N_\ell)^* \qquad \text{Eq. 49}$$

The ionizing radiation has also been diluted so that the photoionization rate from level i is given by

$$R_{i\kappa} = WR_{i\kappa}^* \qquad \text{Eq. 50}$$

The ionization can be divided into the part due to the ground and that due to excited levels so that the ionization balance is given by

$$N_e N^+ \alpha_T = N_1 R_{1\kappa} + \sum_{i>1} N_i R_{i\kappa} \qquad \text{Eq. 51}$$

where α_T is the total recombination coefficient to all levels, and

$$\alpha_T \propto T_e^{-\frac{1}{2}} \qquad \text{Eq. 52}$$

where T_e is the local electron temperature. If we assume that ionization from excited levels dominates that from the ground, Equations 48,50, 51, and 52 can be combined to yield

$$N^+/N_1 = (T_e/T_p)^{\frac{1}{2}} W^2 (N^+/N_1)^* \qquad \text{Eq. 53}$$

where T_p is the photospheric temperature. We see that the dilution factor enters twice, once in the excitaton and once in the ionization. To see the size of the effects these factors produce, Table IV lists W, W^2, and, for the non-isothermal case, $(T_e/T_p)^{\frac{1}{2}}$ and $W^2(T_e/T_p)^{\frac{1}{2}}$ as a function

TABLE IV

Factors Affecting Ionization

r	W	W^2	$(T_e/T_p)^{1/2}$	$W^2(T_e/T_p)^{1/2}$
1.0	.50	.250	1.00	.250
1.1	.29	.085	.85	.072
1.2	.22	.050	.74	.037
1.3	.18	.033	.66	.022
1.4	.15	.023	.60	.014

of r for the radii considered here. Although significant effects in the ionization and excitation can occur, ionization increases outward due to the rapidly decreasing electron density.

One of the assumptions used in determining the atomic densities at the photosphere at maximum light was that the electron densities at that time decreased with increasing radius like the atomic densities, i.e. $N_e \propto r^{-7}$. This is certainly true for our models of Type II envelopes over the range of r considered. The photospheric temperature at maximum light is T_p = 25,000 K. Thus, hydrogen is fully ionized throughout the envelope even considering the ionization to follow Equation 53. Since solar abundance is assumed, hydrogen contributes the bulk of the electron density and N_e does decrease as the atomic density. For Type I envelopes, similar arguments apply for the solar abundance model and the model without hydrogen. However, in the model without hydrogen and helium, it is not a priori clear how the mix of metals should affect the electron density. To see how valid the assumption was in this case, the power of radius by which the electron density fell was calculated by assuming

$$N_e(r) = N_e(r=1)r^{-m} \qquad \text{Eq. 54}$$

and finding m from the actual electron densities calculated by the algorithm mentioned in Chapter III. For the non-isothermal case where the largest effect would be expected, we find that m = 7.1, 7.1, 7.0 and 7.0 for r = 1.1, 1.2, 1.3, and 1.4 respectively. Therefore, the assumption was valid in all cases considered.

Now the predicted populations based on Equations 48, 49 and 53 could be calculated and compared with those obtained from the rate equations. However, there is a more useful form for the results. The contribution a line transition makes to a spectrum is its profile, i.e. the relative amounts of emission and absorption as a function of frequency. For the Sobolev method, Castor [1970] has derived an expression for the line profile in terms of the line source function and the line optical depth. The profile can be described as consisting of an emission part minus an absorption part. The absorption part depends on the line optical depth while the emission part depends on both the line optical depth and the source function.

From Equation 25, we see that $_u$ is roughly proportional to the population of the lower level of the line since, for the most part, the upper level population will be decreased at least by the Boltzmann factor. Looking at Equation 28 and ignoring stimulated emission, we see that S_u is proportional to the ratio of the upper and lower level populations.

If we now assume that Equations 48 and 53 give the population of the lower level of a line of interest and that Equation 49 then gives the population of the upper level, we can write

$$_u{}' = \frac{e}{mc} f_u N' \left(1 - W\frac{g\,N_u^*}{g_u N^*}\right) \Big/ \left(\frac{u}{c}\,\frac{V(R)}{R}\right) \qquad \text{Eq. 55}$$

and

$$S_u{}' \quad WS_u{}^* \qquad \text{Eq. 56}$$

where the primes refer to the predicted values and * again refers to the LTE values at the photospheric temperature. For LTE populations, the line source function is equivalent to the blackbody intensity in the line, so

$$S'_{u\ell} = WB_\nu(T_p) \qquad \text{Eq. 57}$$

In a different fashion Castor [1970] showed that for an unsaturated, radiation dominated line in an expanding atmosphere,

$$S_{u\ell} \approx WI_p \qquad \text{Eq. 58}$$

which reduces to Equation 57 for our assumed photospheric radiation. For the discontinuous opacity case, we would simply predict the line optical depths and source functions to be due to the LTE populations.

Now we will compare the calculated and predicted quantities in the form of ratios of S/S' and τ/τ'. The dilute model results will be presented first followed by those for the discontinuous opacity.

Dilute Models

The simplest physical model considered was the dilute, isothermal model. Some preliminary results have been published [Feldt, 1979] for Si II in Type I envelopes of this sort. We have a choice of chemical compositions here and will look at the results for the case of no hydrogen or helium. The effect of varying chemical composition will be discussed later. The physical processes involved will be discussed in some detail for this case, since, as we shall see, they will be important in all the dilute models.

Figures 4 and 5 show S/S' for the λ6355 and λ4130 lines of Si II as functions of time and fractional radius. The plotted numbers refer to the times relative to maximum light previously indicated in Table III with '1' referring to $t-t_0$ = 5 days and '7' referring to $t-t_0$ = 25 days. We see that, at the earliest times, the predicted source function is increasingly too small as r increases. This is because the upper levels

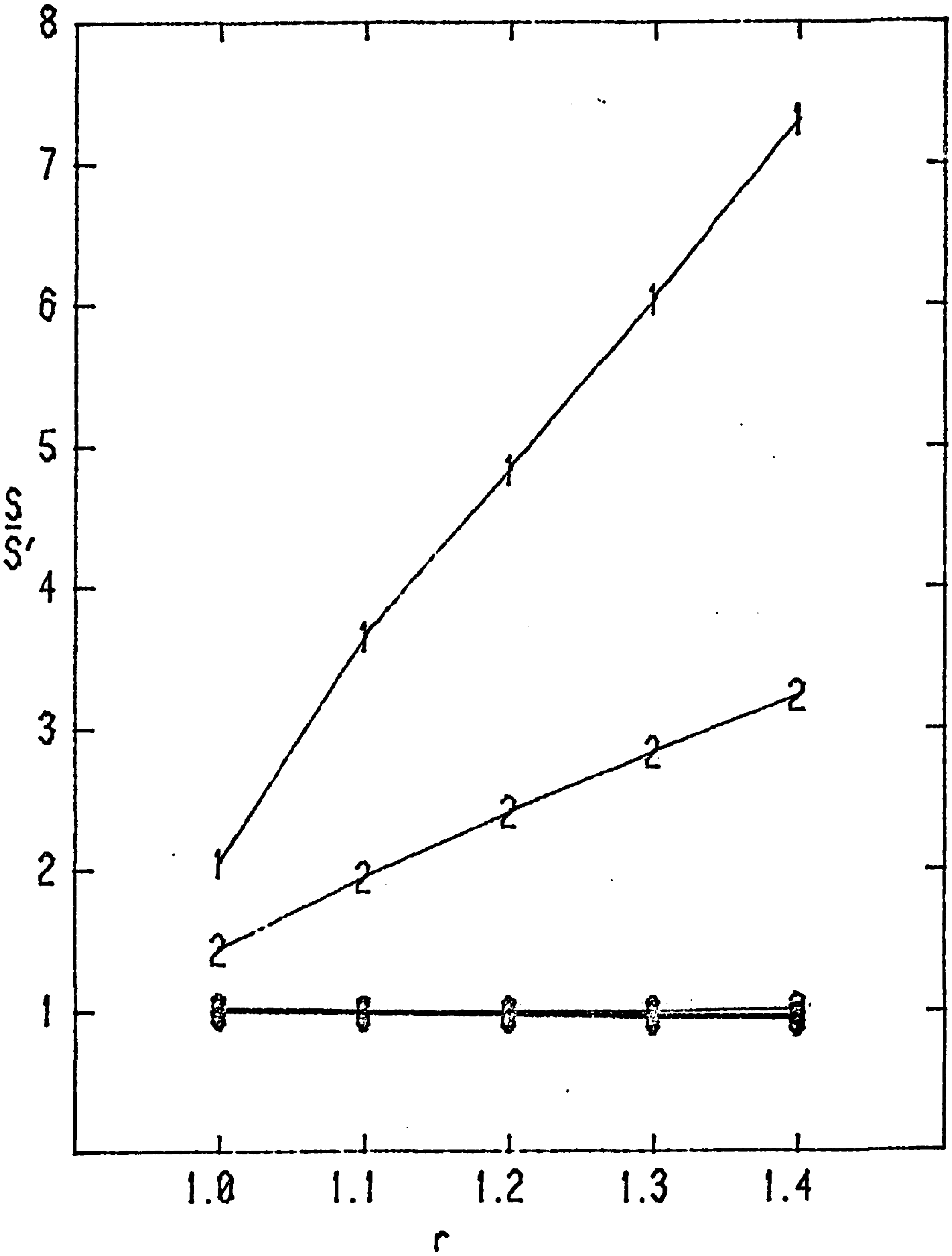

Figure 4. Si II λ6355, isothermal, xH,He

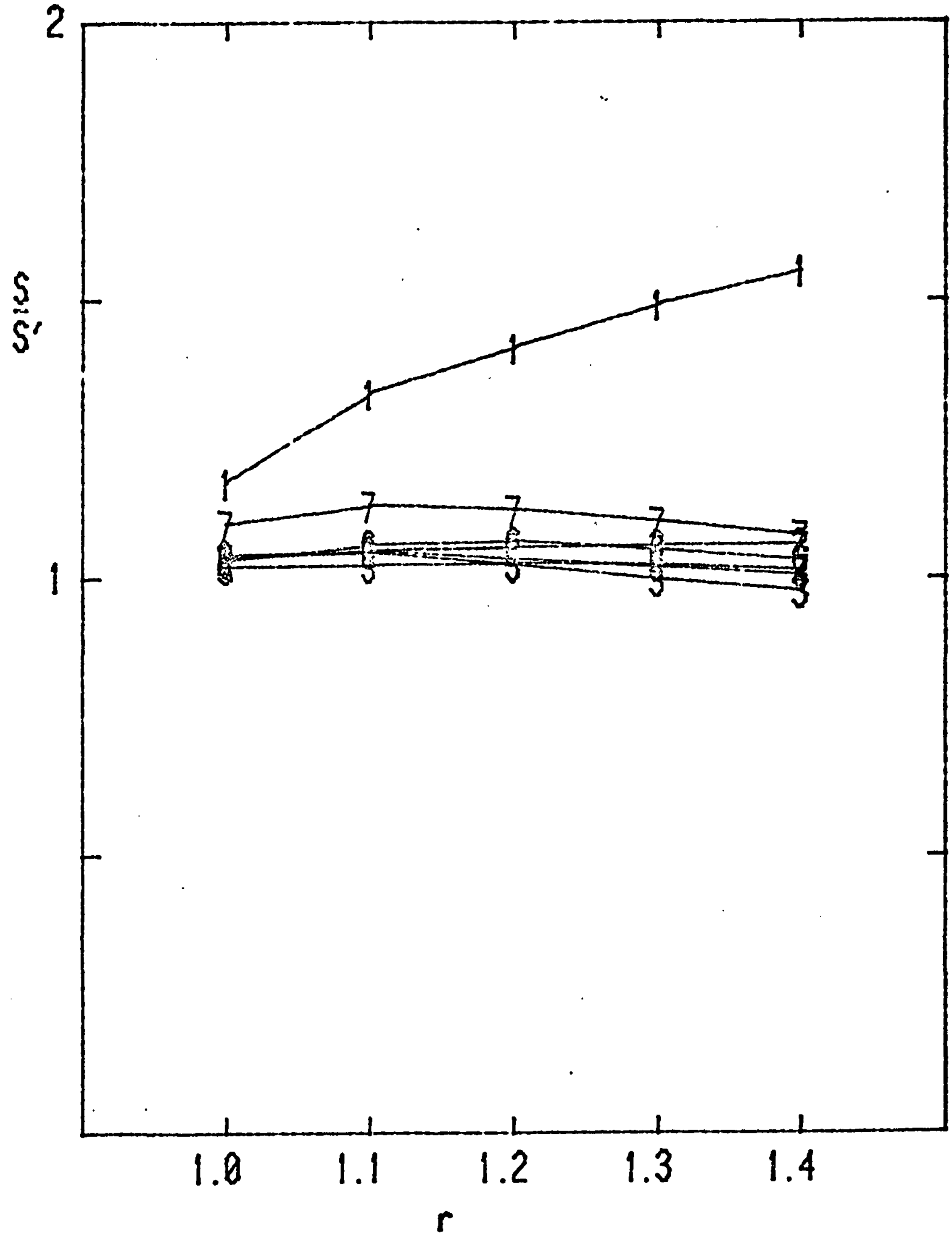

Figure 5. Si II λ4130, isothermal, xH,He

($4p\ ^2P^0$ and $4f\ ^2F^0$) of the transitions are mainly populated by cascades from levels which are populated directly from the ground due to the high temperatures at those times. Thus, the dilution factor enters only once in populating both the lower and upper levels of the transition and so the source function is not proportional to the dilution factor as predicted. The effect is not as strong for the λ4130 transition. This may be due to the larger energy of the $4f\ ^2F^0$ level or to the lack of enough higher ^2D levels which could cascade into it. The effect disappears as the temperature drops, decreasing the ultraviolet radiation field, which in turn, decreases the direct excitation of the upper levels. The upper levels for these lines then do become populated by the lower levels and S/S' drops to unity.

At later times, there is a slight decrease in S/S' with increasing r due to the Doppler shift of the radiation in the line from the photosphere. This was not considered in the prediction and is not a major effect. Since a point in the envelope is moving away from the photosphere, the radiation received in the line at frequency ν was originally at frequency $\nu_D = \nu(1 + \frac{\Delta V}{c})$ where ΔV is the velocity difference and is at most $\sim .01$ for the radii considered. Thus, the radiation in the line from the photosphere is changed by the factor B_{ν_D}/B_ν, where B_ν is the blackbody intensity. For the low temperatures at later times, this ratio is roughly given by

$$B_{\nu_D}/B_\nu = (\nu_D/\nu)^3 \exp[h(\nu - \nu_D)/kT_p] \qquad \text{Eq. 59}$$

which is increasingly less than unity as r, and thus ΔV, increases.

Figures 6 and 7 show τ/τ' for the same two lines in this model.

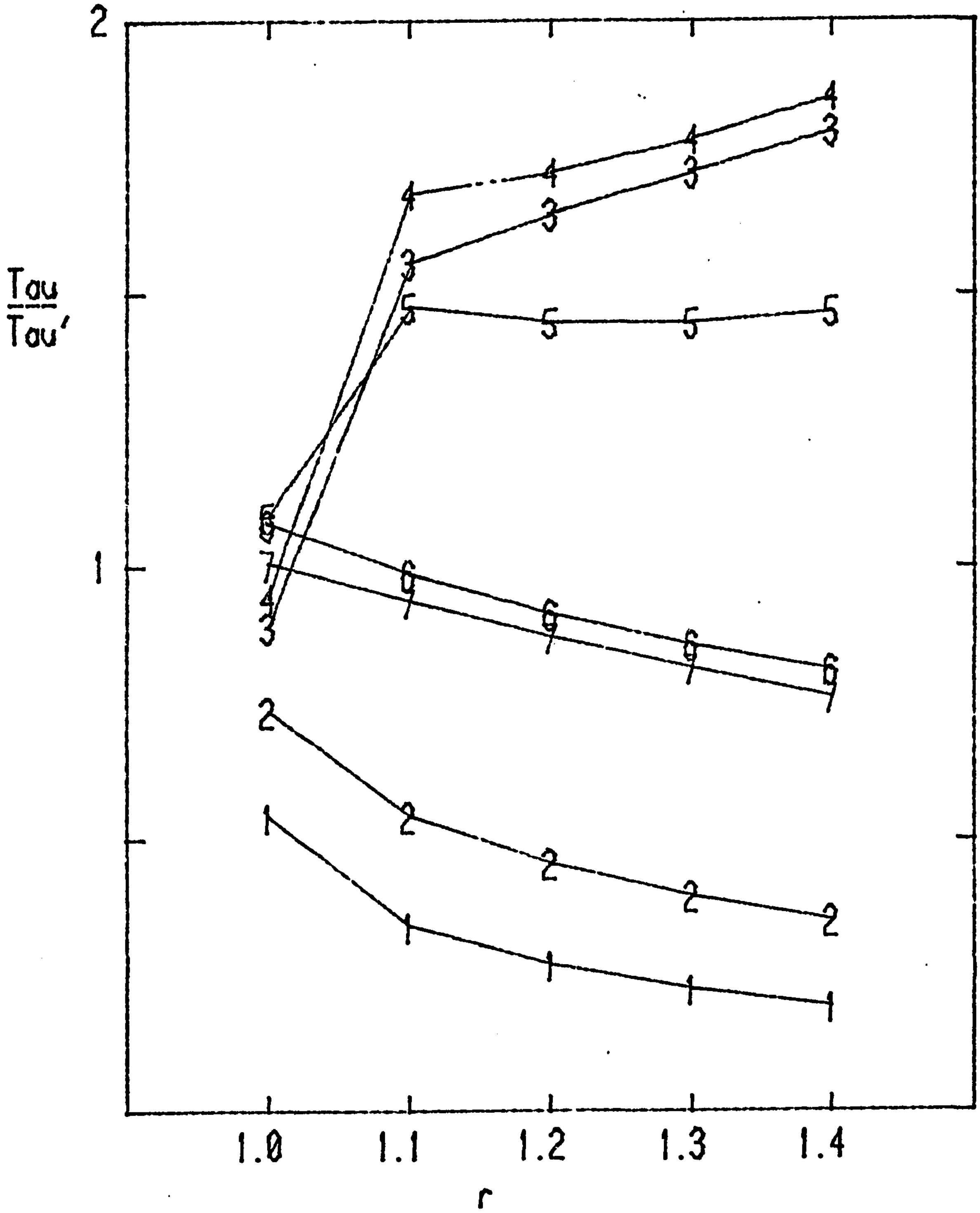

Figure 6. Si II λ6355, isothermal, xH,He

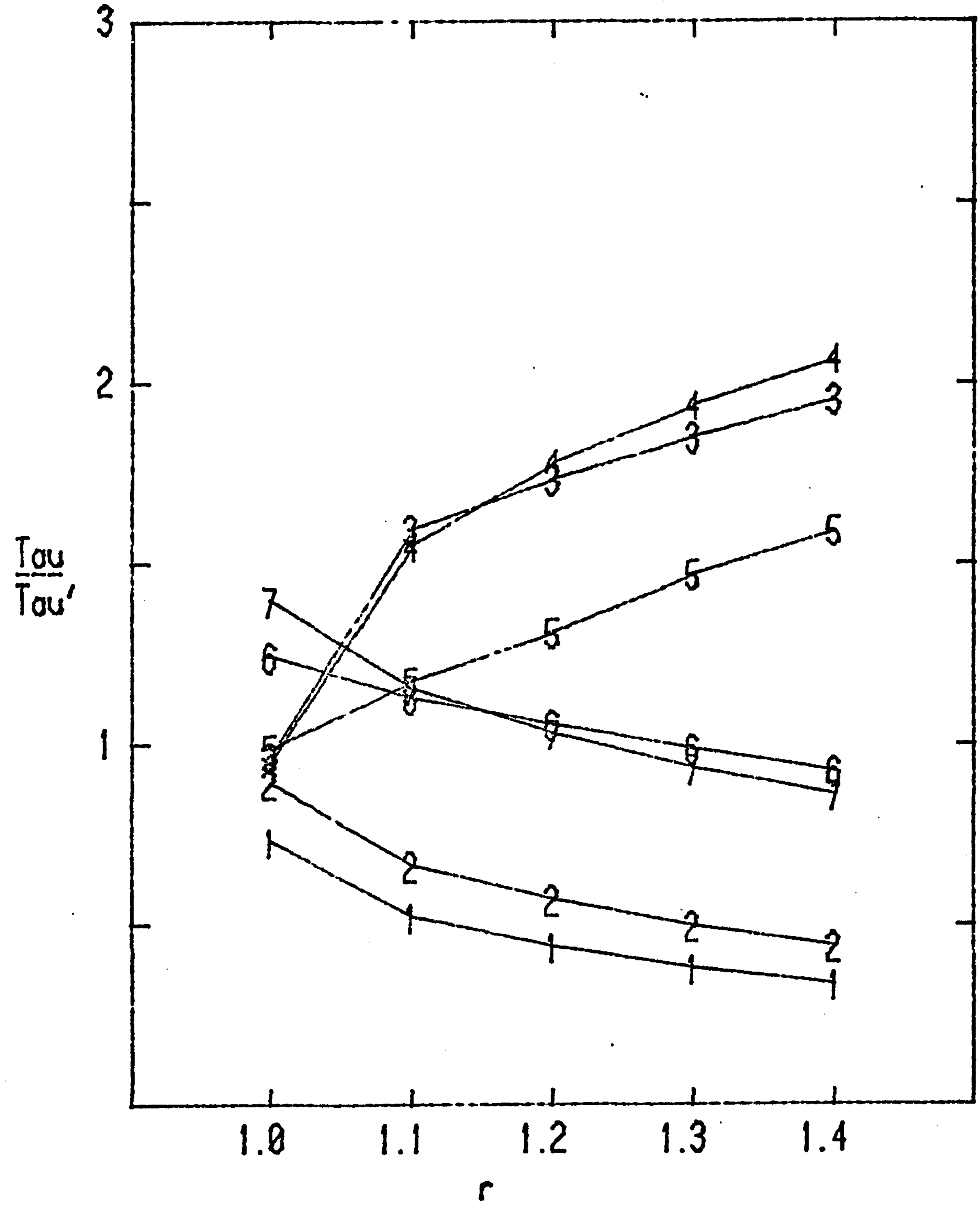

Figure 7. Si II λ4130, isothermal, xH,He

At the earliest times, the predicted τ are too large and increasingly so as r increases. This is due to the breakdown of the assumption that the ionization from the ground level is insignificant. It actually contributes about 40% of the ionization at those times so that the ionization is roughly proportional to $W^{1.4}$ instead of W^2 since the dilution factor enters ionization from the ground level only through the photoionization rate. The result is that the ionization is greater than predicted and, since the higher ionization stages of Si are dominant at these times, the density of Si II is less. This decreases all line optical depths.

At intermediate times, the predicted τ are too small and increasingly so as r increases. By these times, the cooling envelope has decreased the ionization enough so that, even though Si III is the dominant ion, the ground level population of Si II is large enough to cause the ground continuum to become optically thick. This means that the ionizing radiation must come from excited levels. Many of these levels are populated as described by Equation 49 so that some fraction of the ionizing radiation has effectively been diluted three times rather than twice. Thus, the actual ionization is less, and all line strengths are greater, than predicted. This does not occur at r=1 since the continuum optical depth is assumed to be zero there.

The reason τ/τ' increases with increasing radius at these intermediate times is due to the effect of the Doppler shift, similar to that described earlier. However, here the effect is in the continuum radiation and is much larger. From Equations 16, 20, and 29 and using the ν^{-3} dependence of the photoionization cross-sections, we see that, for an optically thin continuum, we can form the ratio of photoionization rates

$$R_{2\kappa}^{D}/R_{2\kappa} = \frac{\int_{\nu_D}^{\infty} \nu^{-1}[\exp(h\nu/kT) - 1]^{-1}d\nu}{\int_{\nu}^{\infty} \nu^{-1}[\exp(h\nu/kT) - 1]^{-1}d\nu} \qquad \text{Eq. 60}$$

where the subscript and superscript D refers to the Doppler-shifted case. One of the principle ionizing levels at these times is the $3p^2$ ^2D level, for which the continuum begins at $h\nu \simeq 76,000$ cm^{-1} and, since $kT < 8000$ cm^{-1} here, we find $h\nu/kT > 9$. Therefore, the numerator and denominator of Equation 60 can be approximated by exponential integrals which, in turn, can be approximately evaluated so that

$$R_{2\kappa}^{D}/R_{2\kappa} = \nu/\nu_D\exp[h(\nu - \nu_D)/kT] \qquad \text{Eq. 61}$$

Allowing the frequency to be increased one percent by the Doppler shift and inserting the appropriate temperatures and frequency, we see that at r=1.4, this ratio can be as low as .85 for $t-t_0 = 10$ days and as low as .75 for $t-t_0 = 25$ days. The main reason the lines are not as greatly affected as the continuum is that $h\nu$ is much smaller for them.

At the latest times, τ/τ' is nearly unity with a slight tendency to decrease with increasing r. Si II is the dominant ion here, and the effects due to ionization differences become minimal. Rather, there is a slight decrease in the excitation (from the ground level) of the lower levels of the transition. (Recall that $\tau_{u\ell}$ is roughly proportional to the population of the lower level.) The energy differences for these excitations are much greater than those in the lines, so the effect is more noticeable than the slight effect found in the source functions. Notice that, as expected, the effect is greater for the higher lying 3d ^2D level associated with the $\lambda 4130$ transition than for the 4s ^2S level associated with the $\lambda 6355$ transition.

If we now look at the source function ratios for hydrogen in a dilute, isothermal model for Type II supernovae, we find little new. Figures 8 through 11 give S/S' for the first four Balmer lines beginning with Hα. The plotted numbers now refer to the times relative to maximum light given in Table II with '1' referring to $t-t_0 = 0$ days. The calculated source functions at early times are not as discrepant from those predicted as was the case for Si II. (Compare Figures 8 and 4.) This is due to the fact that we start the Type I models before maximum light at a temperature which is greater than for the Type II models at maximum light. The lower temperature for the earliest times considered in the Type II models causes less direct population of the upper levels. At late times, S/S' is near unity for Hα. However, for the other Balmer lines, S/S' drops to near one-half. This is due to the influence of levels other than n=2 in populating the upper levels of these lines and allowing the dilution factor to enter more than once. The Doppler shift produces neglible effect for these lines due to the smaller velocity gradient in the Type II envelope.

Figure 12 shows τ/τ' for Hα. Since all Balmer lines depend on the population of n=2 for their line optical depths, it would be redundant to give τ/τ' for the other lines also. We see essentially the same behavior as observed for Si II. For $r > 1$, the only difference found is at late times where τ/τ' does not fall below unity. This is due to the fact that hydrogen is not completely recombined even at

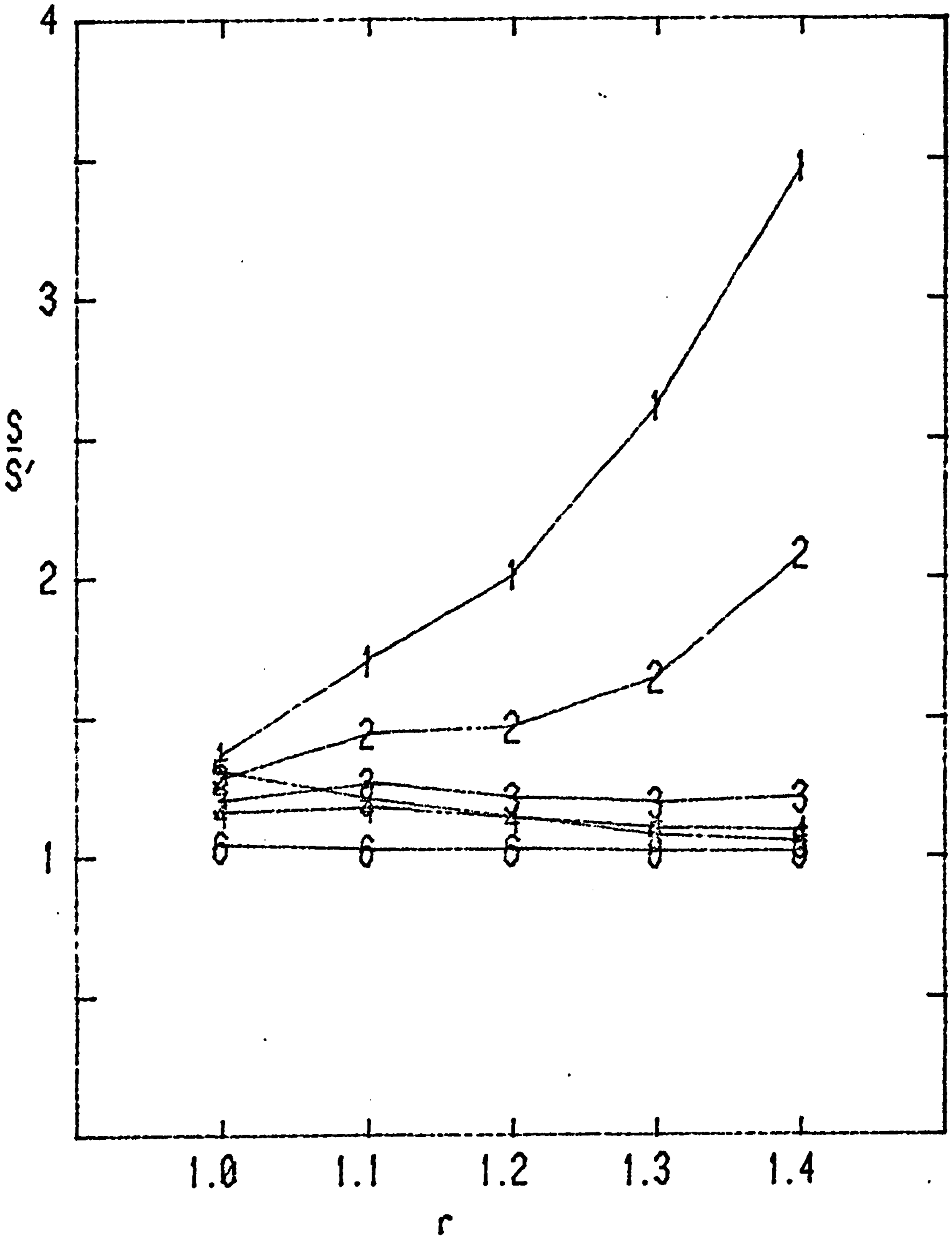

Figure 8. Hα, isothermal

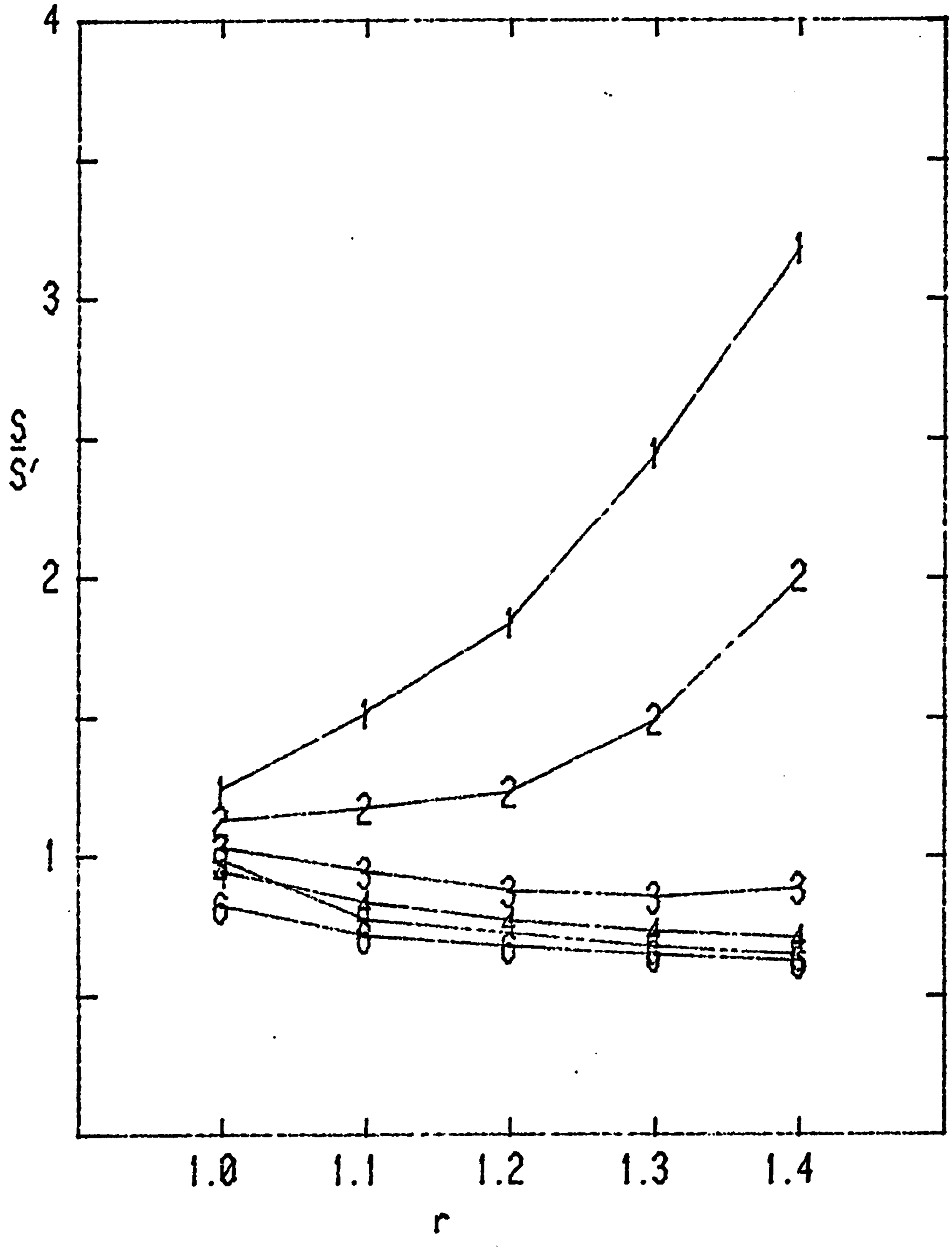

Figure 9. Hβ, isothermal

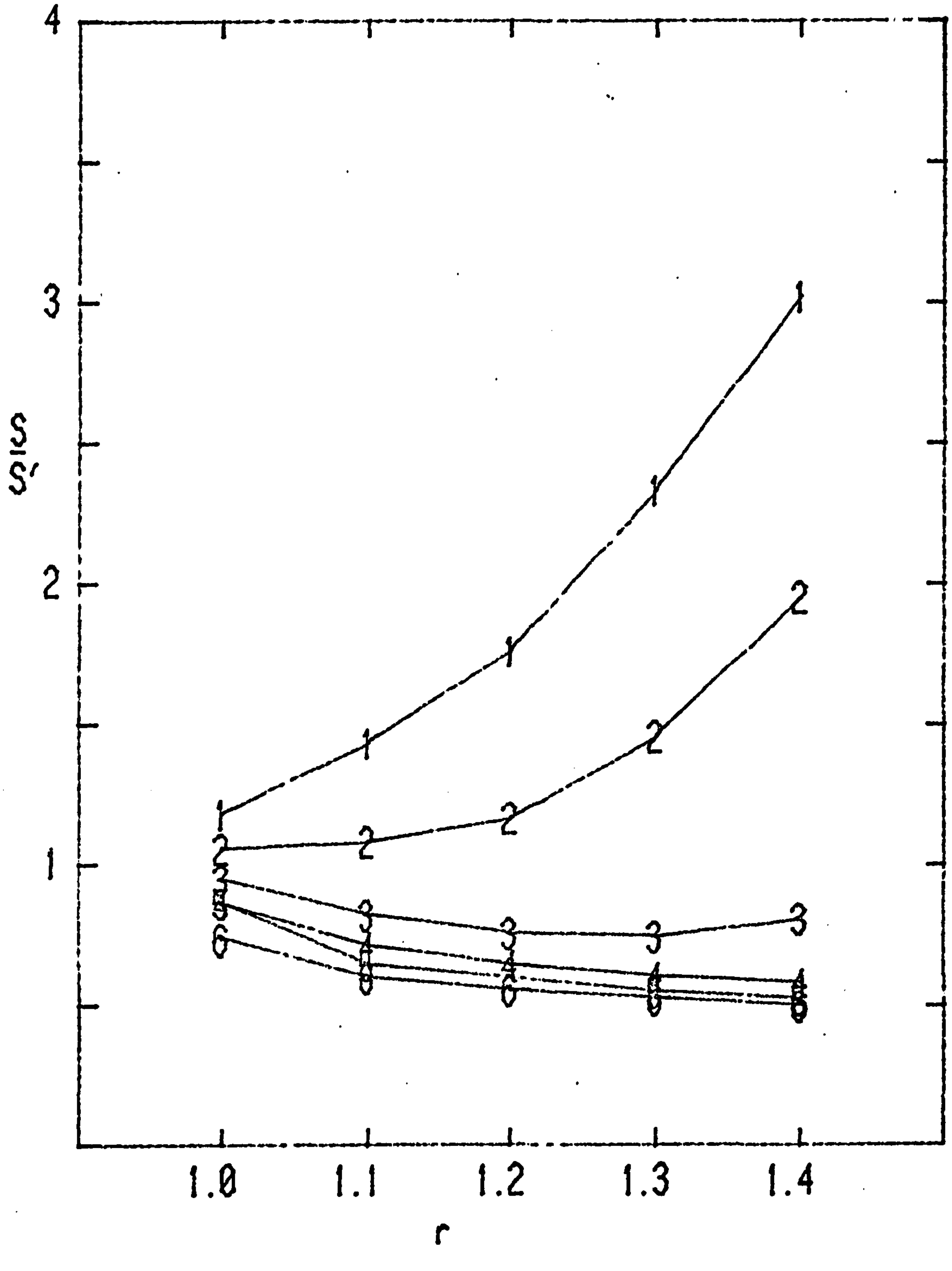

Figure 10. HY, isothermal

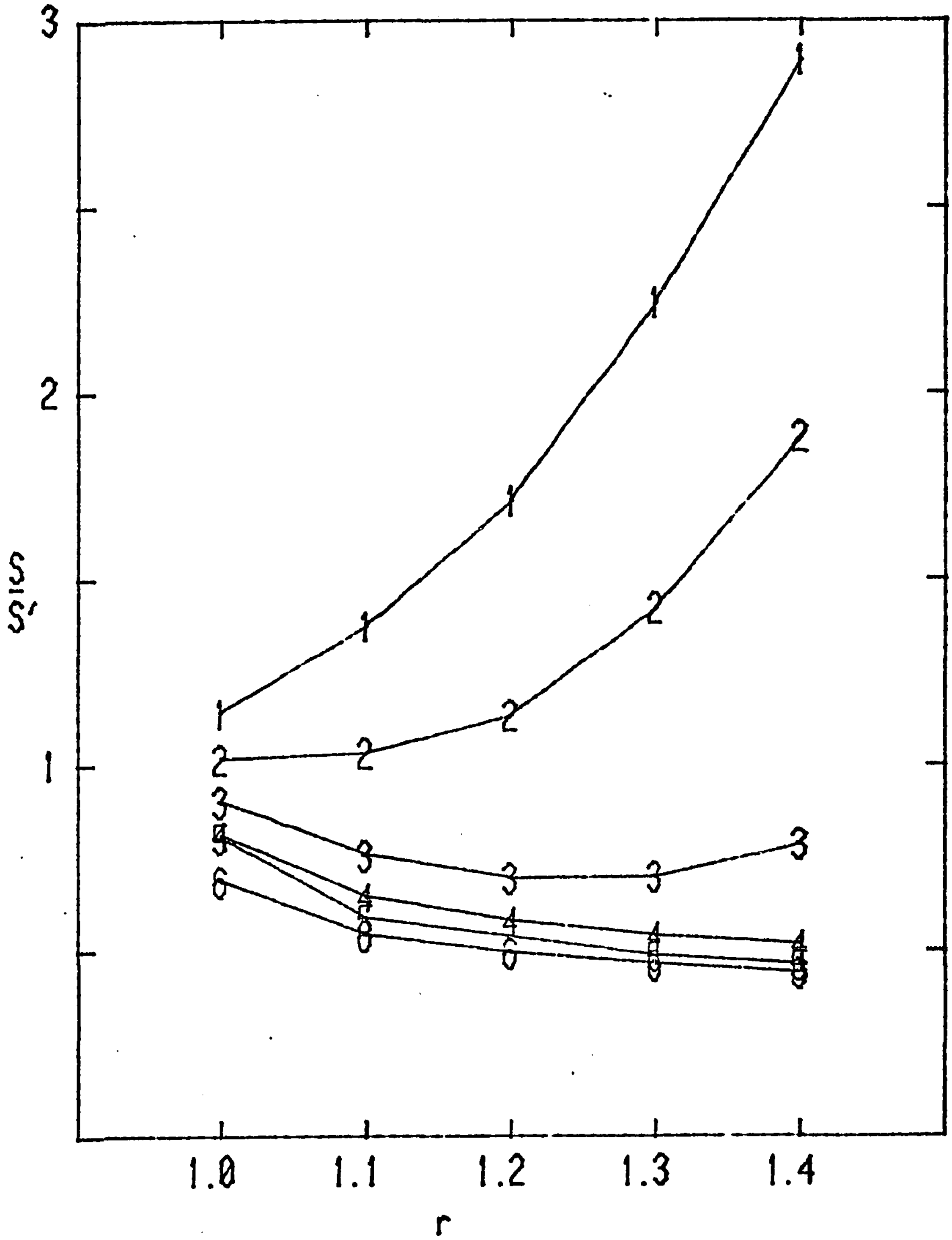

Figure 11. Hδ, isothermal

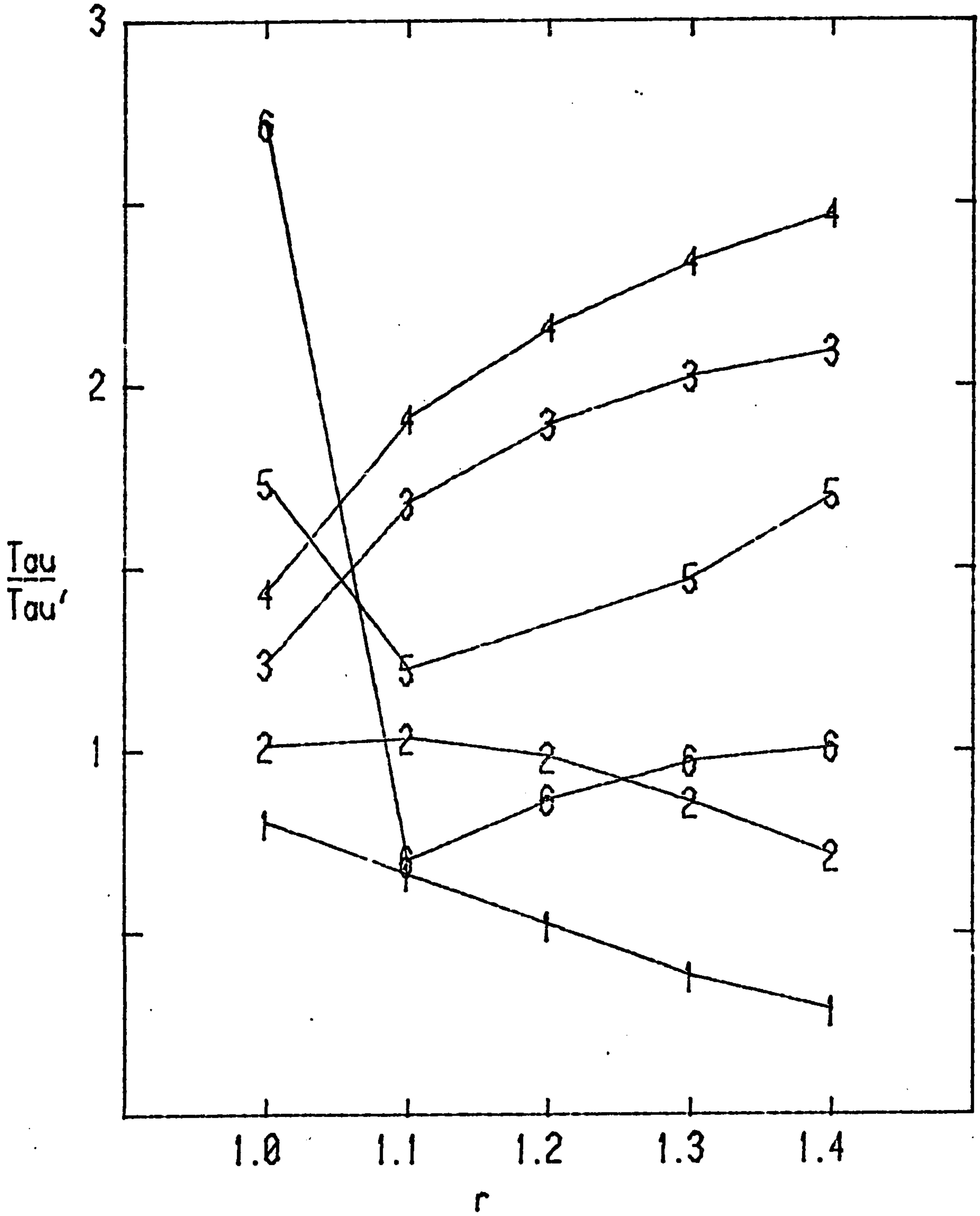

Figure 12. Hα, isothermal

$t-t_0$ = 45 days. Therefore, even though the line excitation is somewhat less than predicted (as described for Si II), this is more than corrected for by the lower ionization at $t-t_0$ = 30 days and the two balance at $t-t_0$ = 45 days. The odd behavior of τ/τ' at r=1 at late times is due to the artificial lack of any continuum optical depth from the ground. This increases the ionization and feeds the n=2 level via recombination and cascades.

Next, we consider the effect of a temperature gradient in the envelope. According to the predictions, it should simply decrease the ionization by $(T_e/T_p)^{1/2}$. Since this is included in the predictions, the ratios S/S' and τ/τ' should not change from the isothermal case unless other physical effects become important. Figure 13 through 21 show the counterparts of Figures 4 through 12 in the case of the temperature gradient given by Equation 9. It is clear by comparison that the same physical processes are important in this case as were for the isothermal one. For hydrogen, numerical difficulties were encountered for $t-t_0$ = 30 days and these results are not available. However, the general agreement with the isothermal case suggests no surprises would have been likely.

For Si II in Type I supernovae, another consideration is the chemical composition of the envelope. As hydrogen and helium are removed from the model, the density of the metals must be increased to maintain the electron densities assumed at maximum light. The strength of the lines is not only affected through the total Si density, but also by the effects of composition on the electron densities as a function of

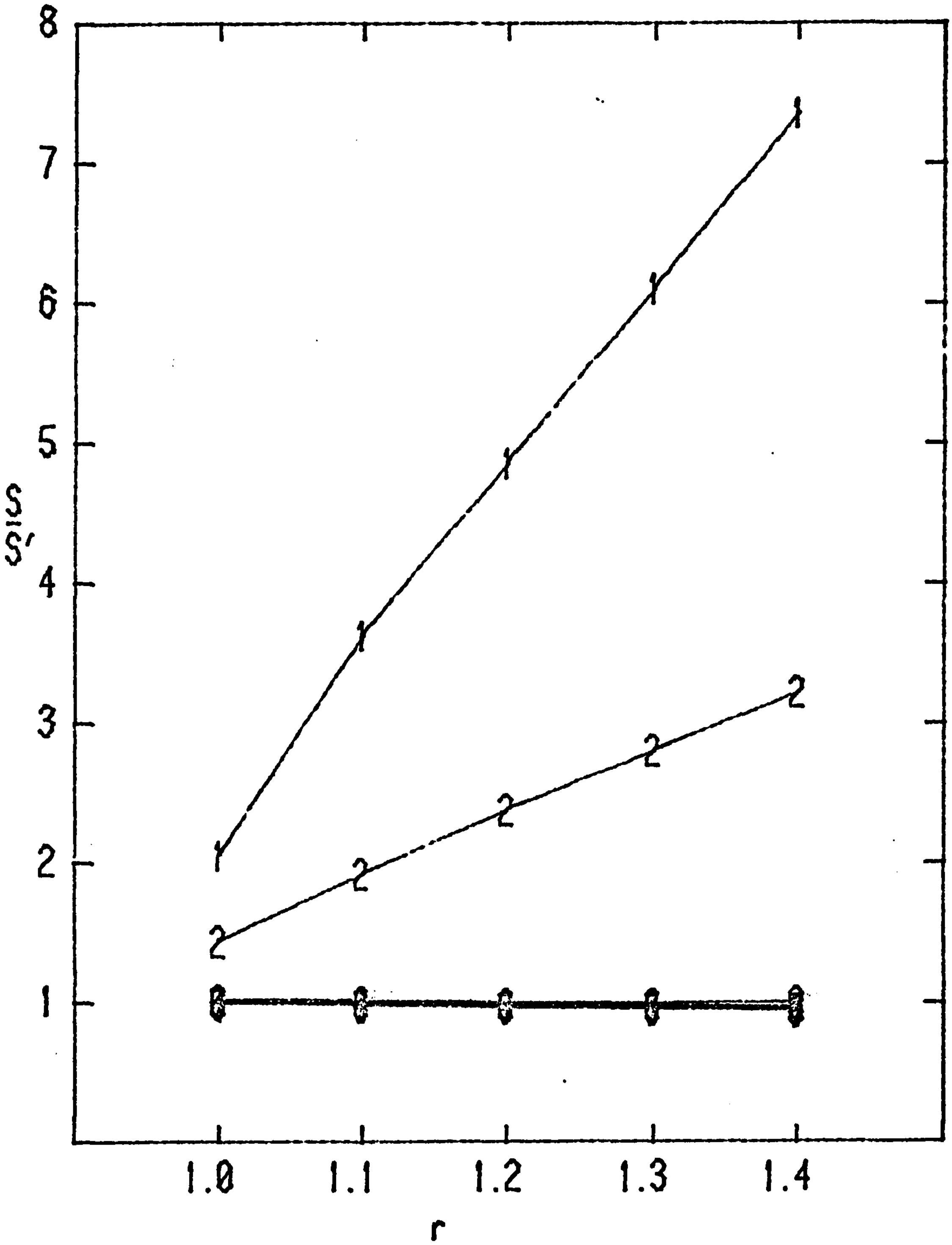

Figure 13. Si II λ6355, non-isothermal, xH,He

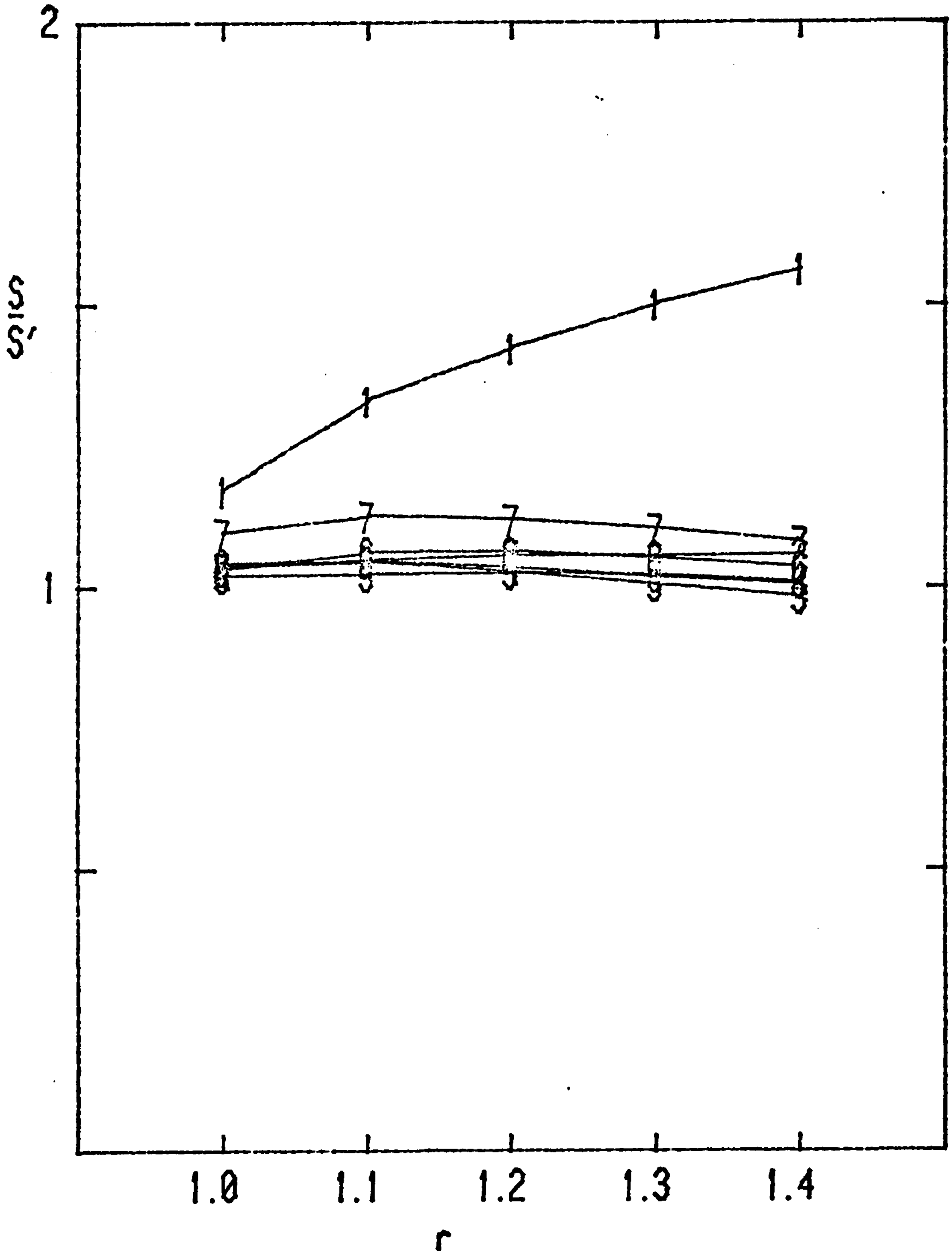

Figure 14. Si II λ4130, non-isothermal, xH,He

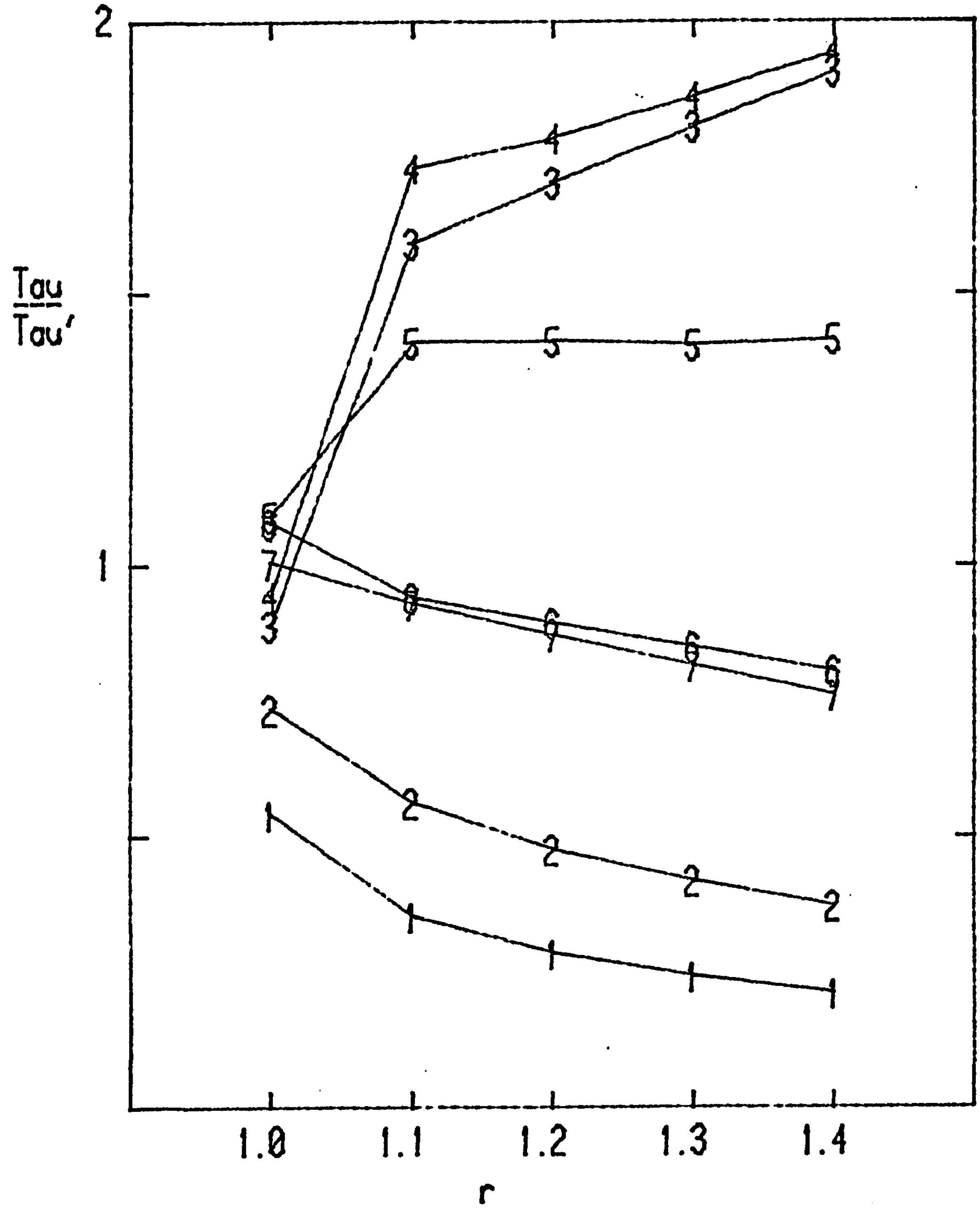

Figure 15. Si II λ6355, non-isothermal, xH,He

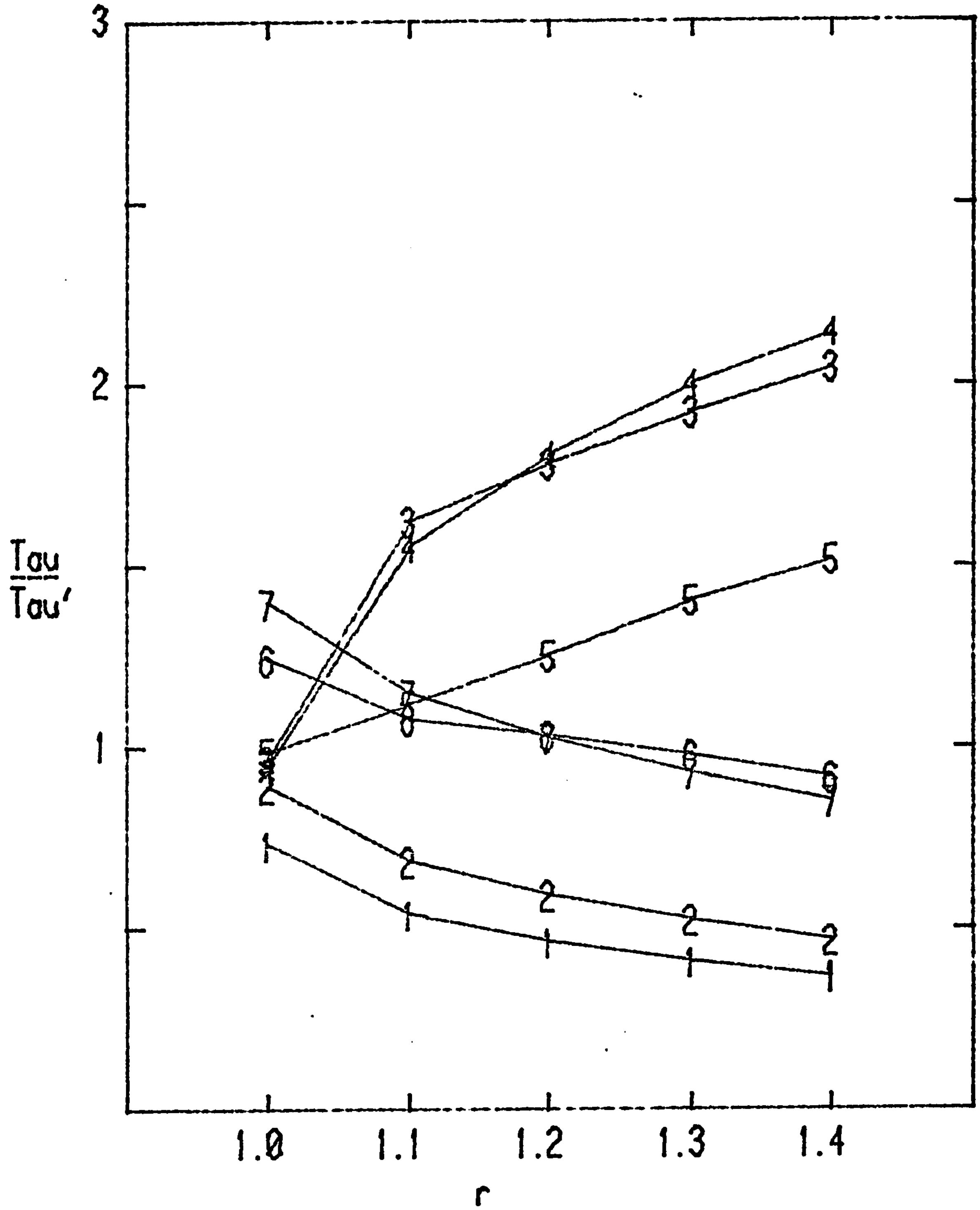

Figure 16. Si II λ4130, non-isothermal, xH,He

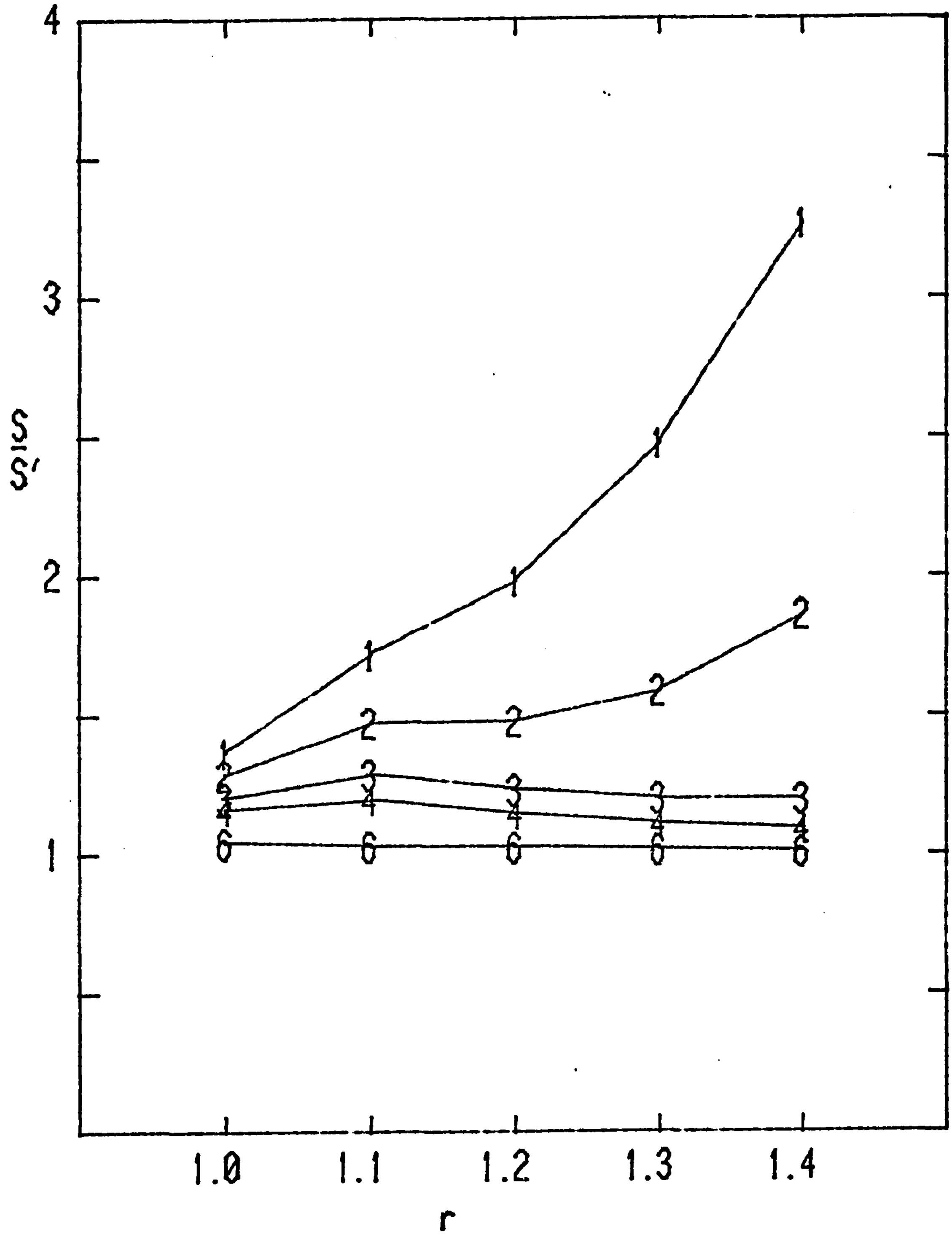

Figure 17. Hα, non-isothermal

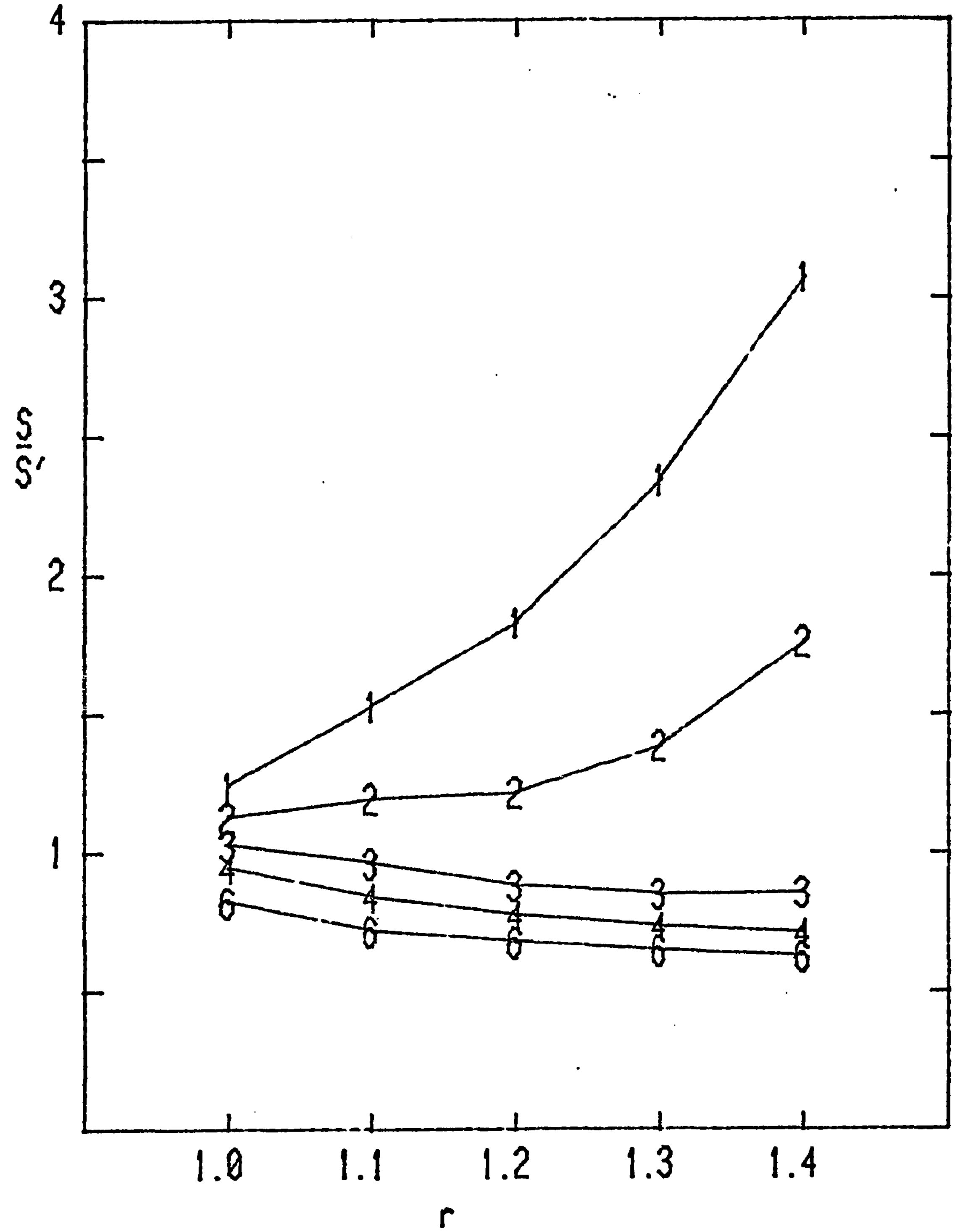

Figure 18. Hβ, non-isothermal

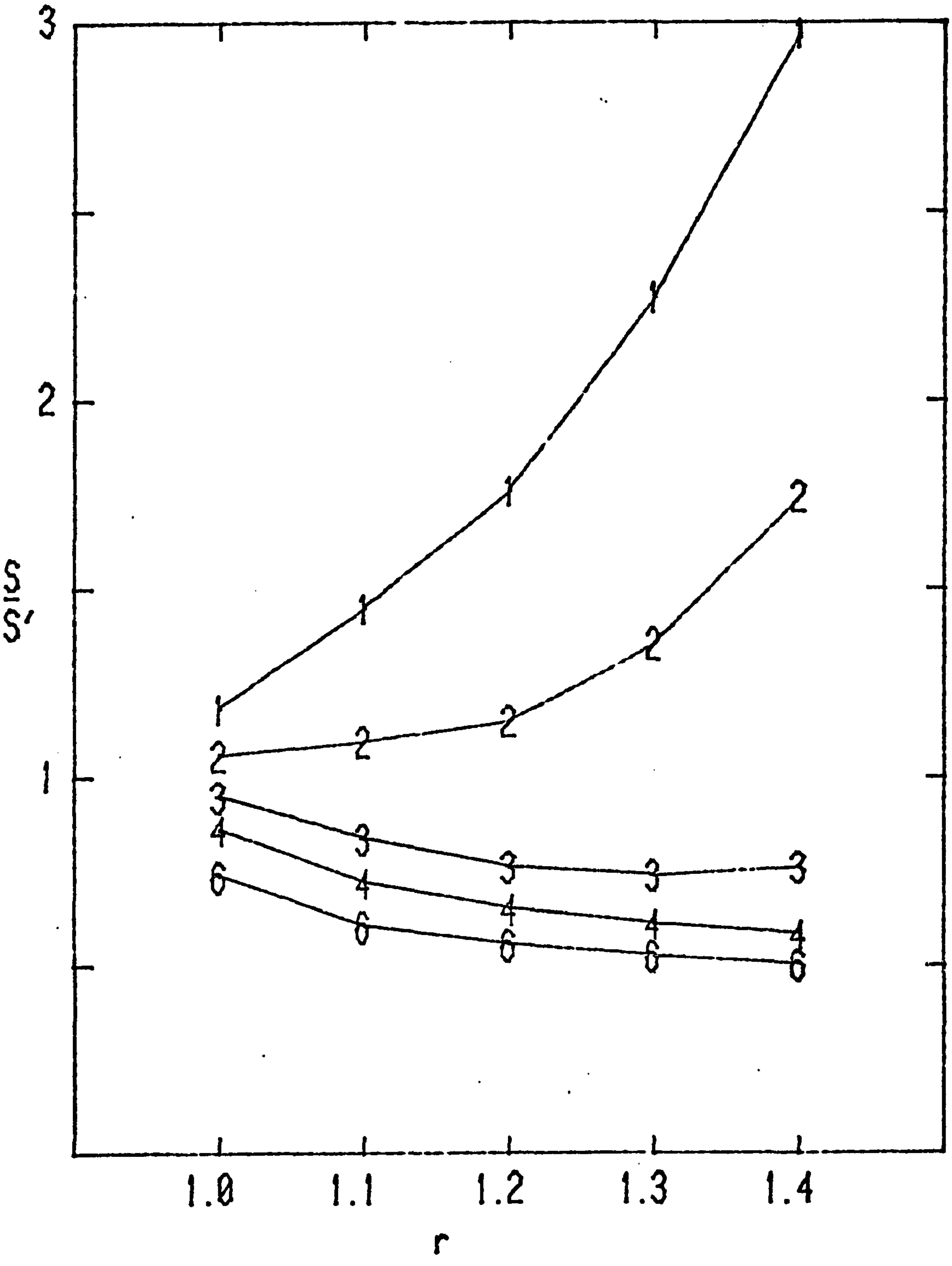

Figure 19. Hγ, non-isothermal

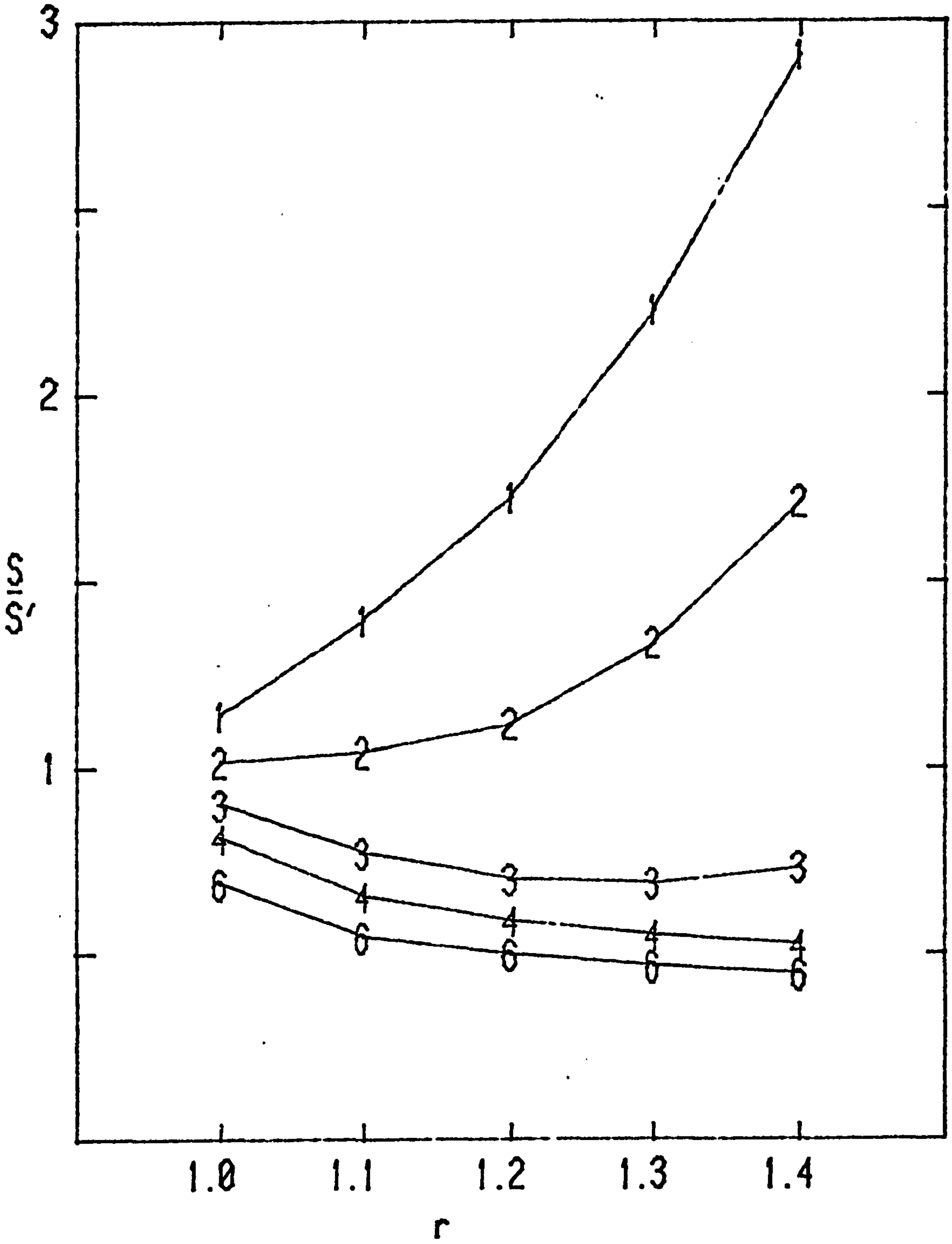

Figure 20. Hδ, non-isothermal

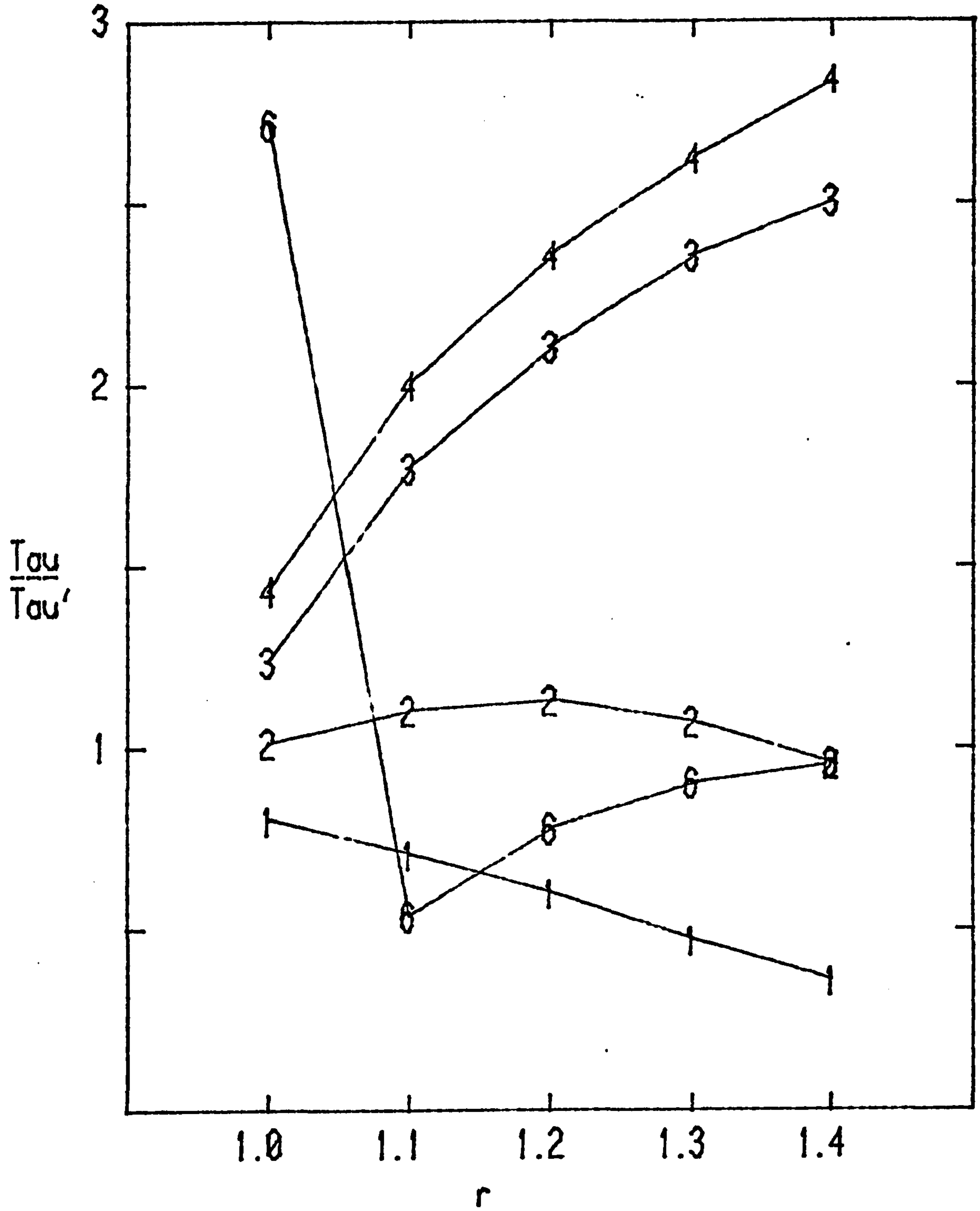

Figure 21. Hα, non-isothermal

time and radius and by changes in the mix of escape probabilities. The electron densities affect the level populations mostly through recombination while a change in the mix of escape probabilities can affect excitation. The effect of varying chemical composition was explored in the non-isothermal models since they are likely to be more realistic.

Figures 22 and 23 give S/S' for the λ6355 and λ4130 transitions in the model with no hydrogen. Figures 24 and 25 show the counterparts for the model with solar abundance, while Figures 13 and 14 show the counterparts for the model without hydrogen and helium. There are very few differences. At the time marked '3' ($t-t_0$ = 5 days), there is some change in S/S' for λ6355 due to a change in the mix of escape probabilities. The upper level ($4p\ ^2P^0$) of this transition is also connected to the $3p^2\ ^2D$ level via a line at 3858 Å. Because the oscillator strength for this transition is smaller than for the λ6355 transition, as the Si density is increased the escape probability for λ6355 decreases before that for λ3858. This means the population of the upper level is more likely to be decreased by the escape of λ3858 photons as the Si density is increased and this decreases the source function. At times before or after this, these two escape probabilities are both large or both small so that this effect does not occur.

The effect of varying chemical composition on the line optical depths, although somewhat more noticeable, is also fairly small. The τ/τ' corresponding to the case without hydrogen and helium shown in Figures 15 and 16 are given in Figures 26 and 27 for the case without hydrogen and in Figures 28 and 29 for solar abundance. Comparing Figures 15,

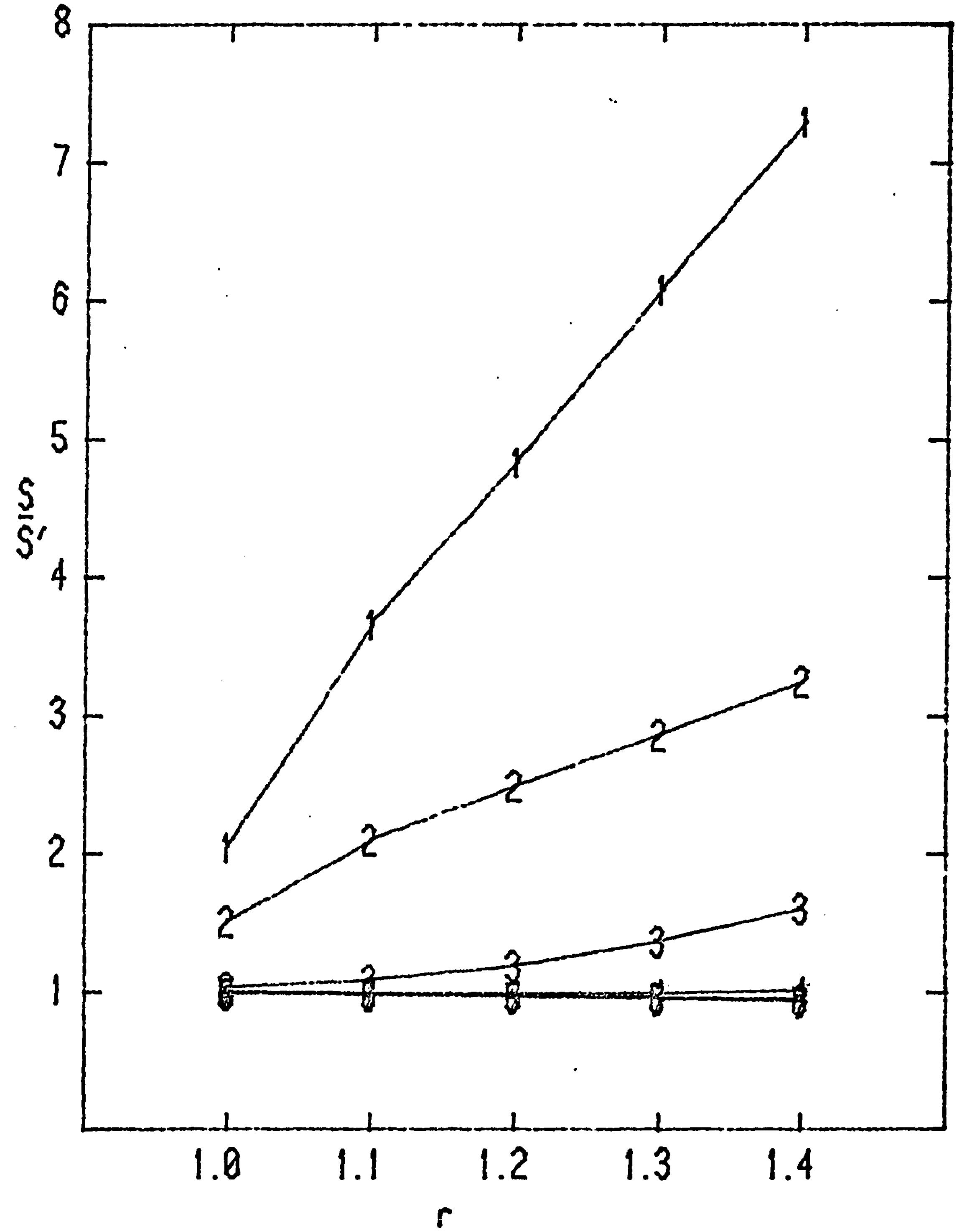

Figure 22. Si II λ6355, non-isothermal, xH

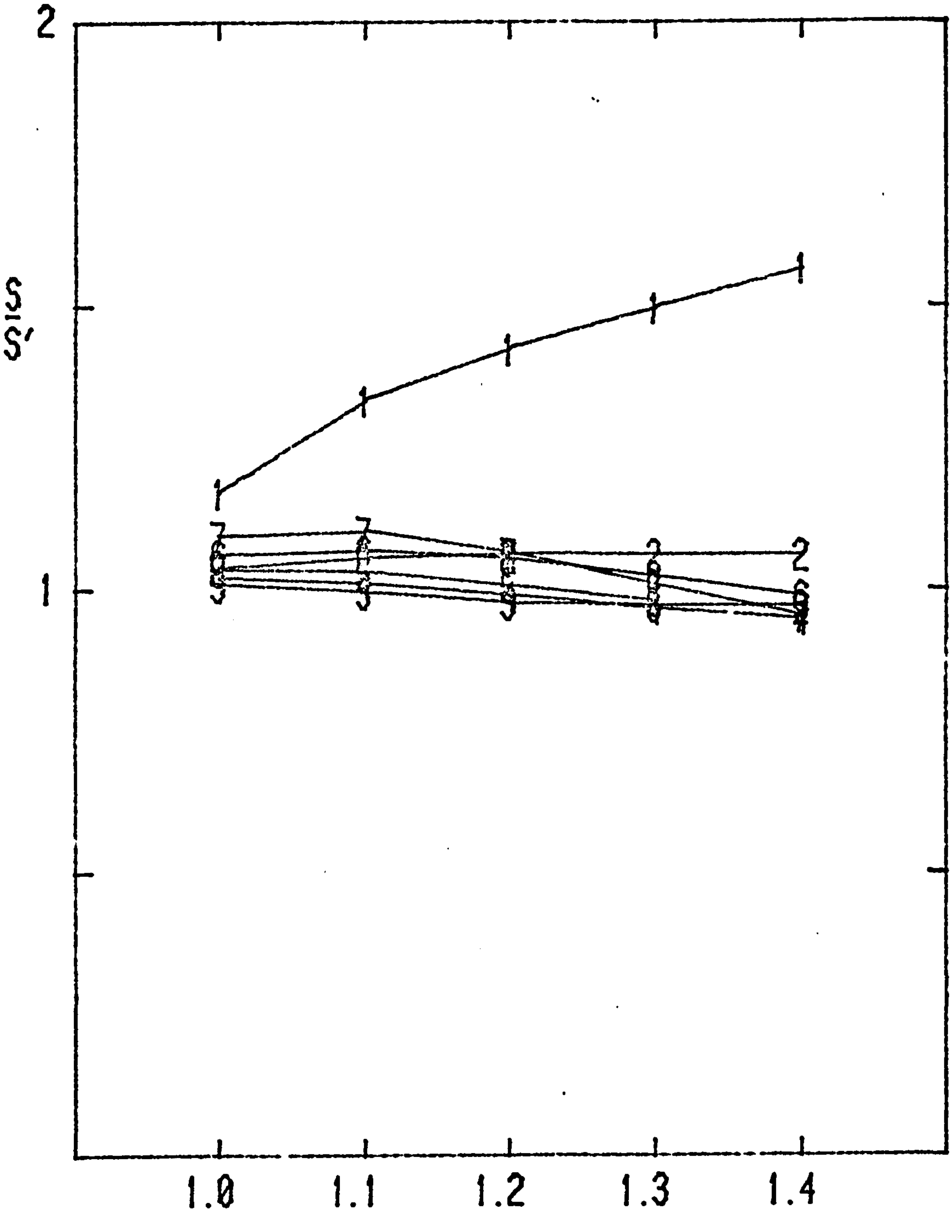

Figure 23. Si II λ4130, non-isothermal, xH

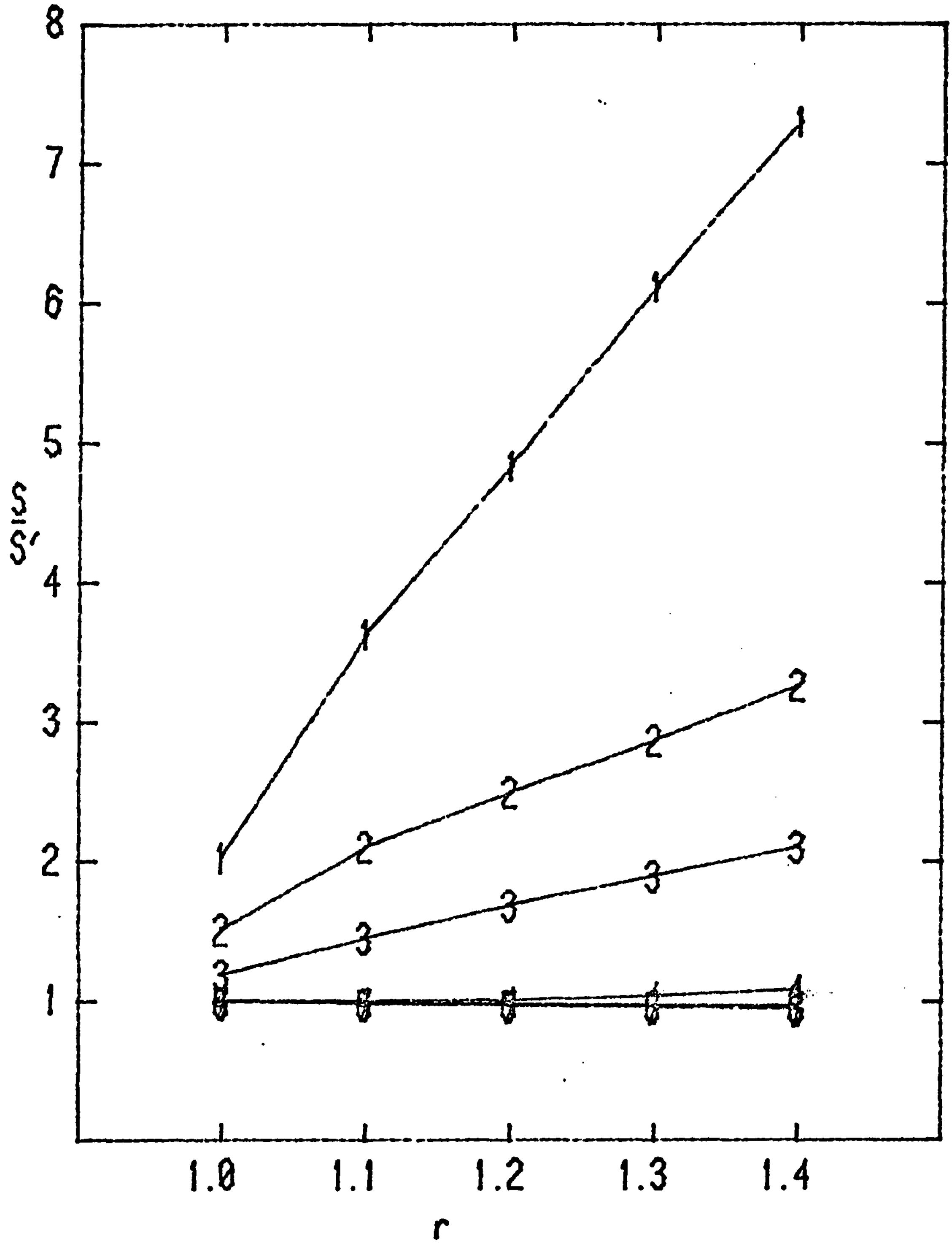

Figure 24. Si II λ6355, non-isothermal, solar

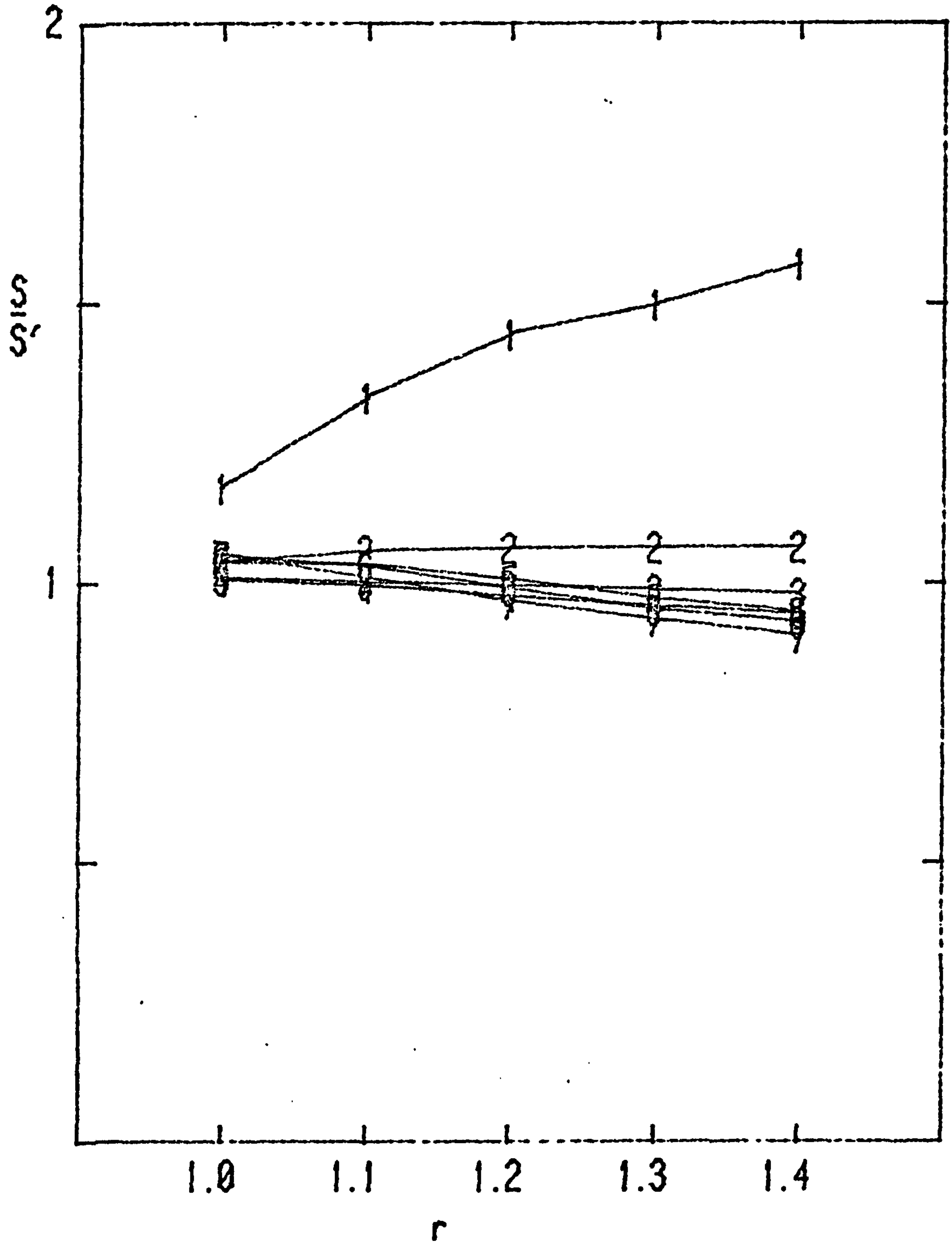

Figure 25. Si II λ4130, non-isothermal, solar

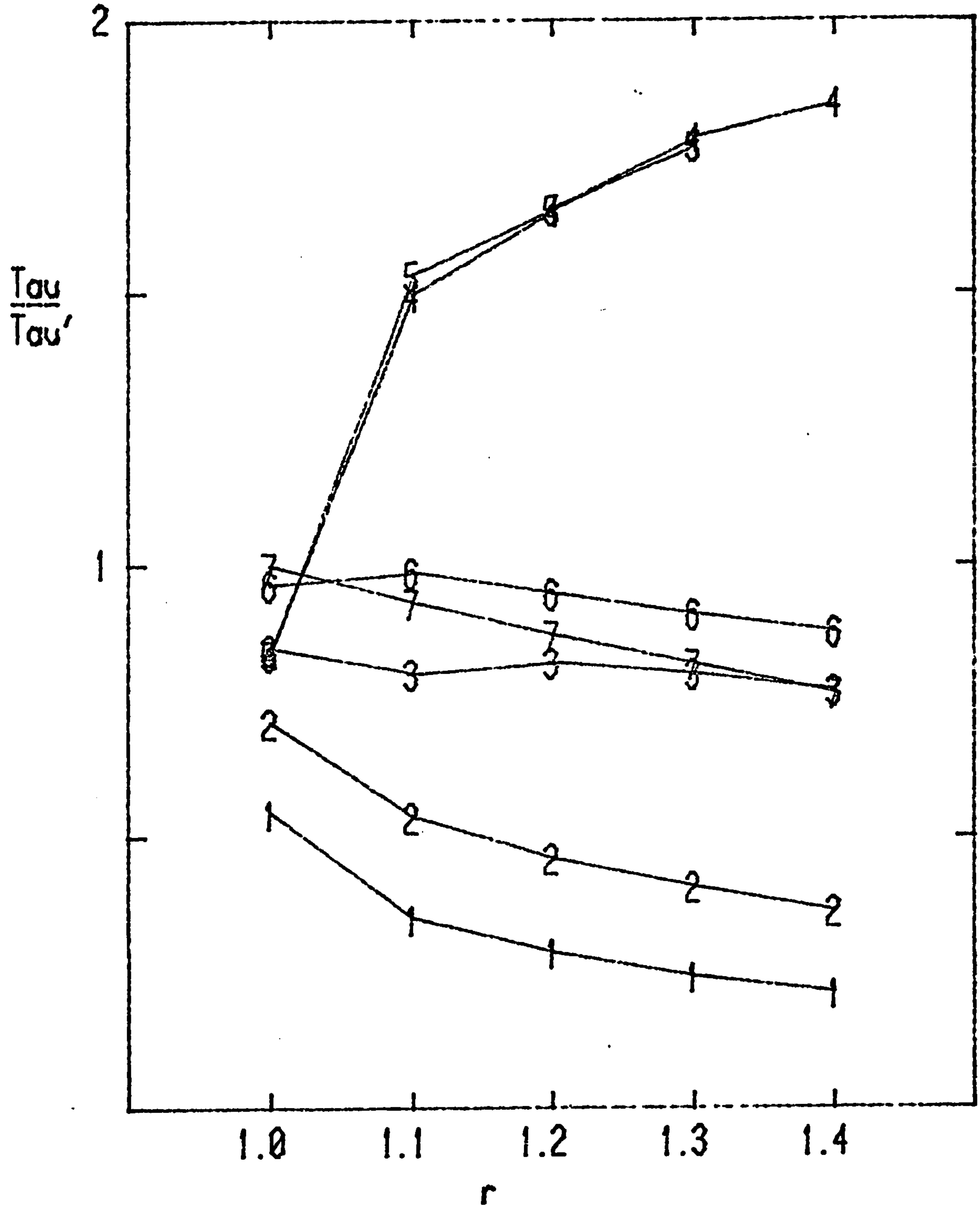

Figure 26. Si II λ6355, non-isothermal, xH

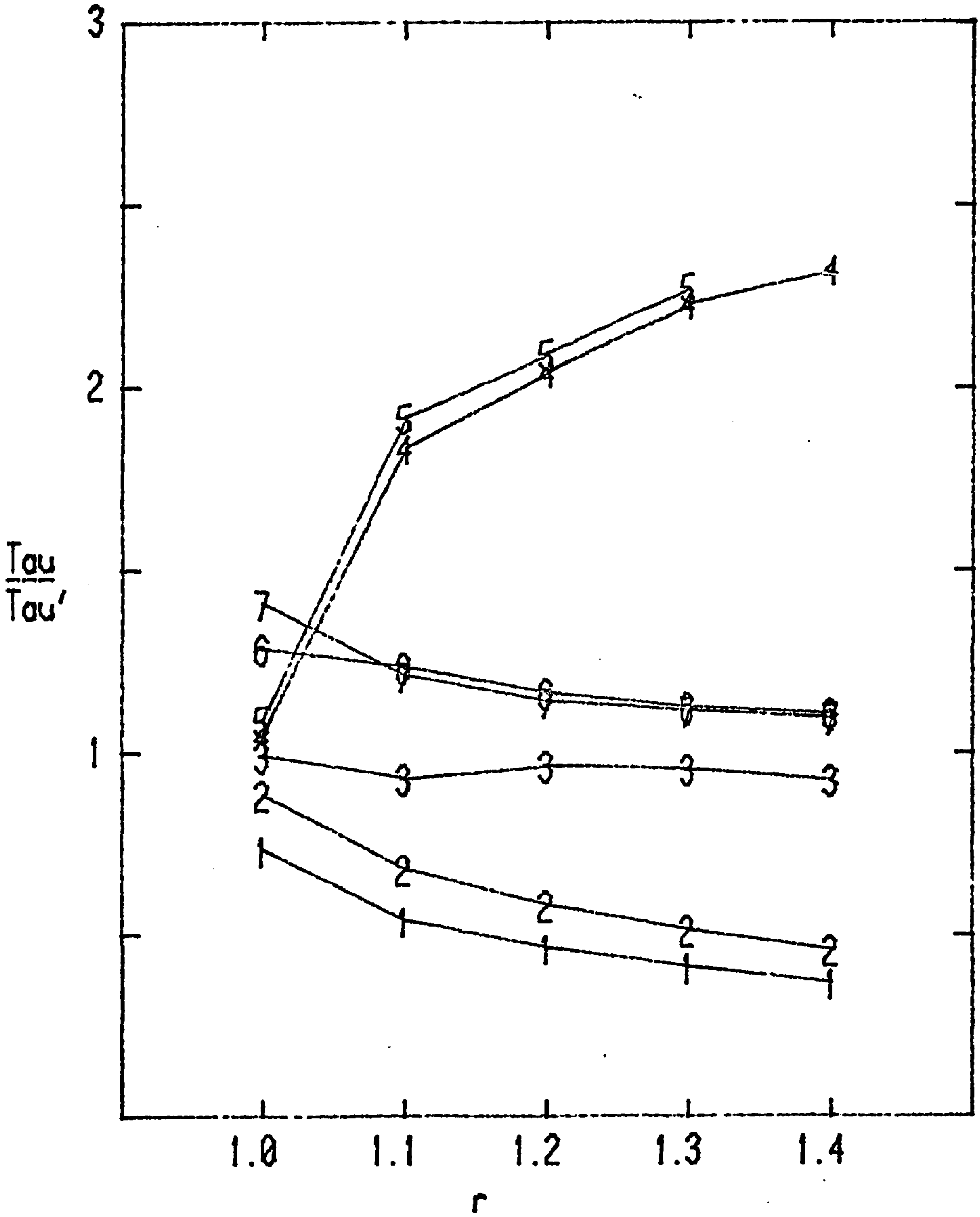

Figure 27. Si II λ4130, non-isothermal, xH

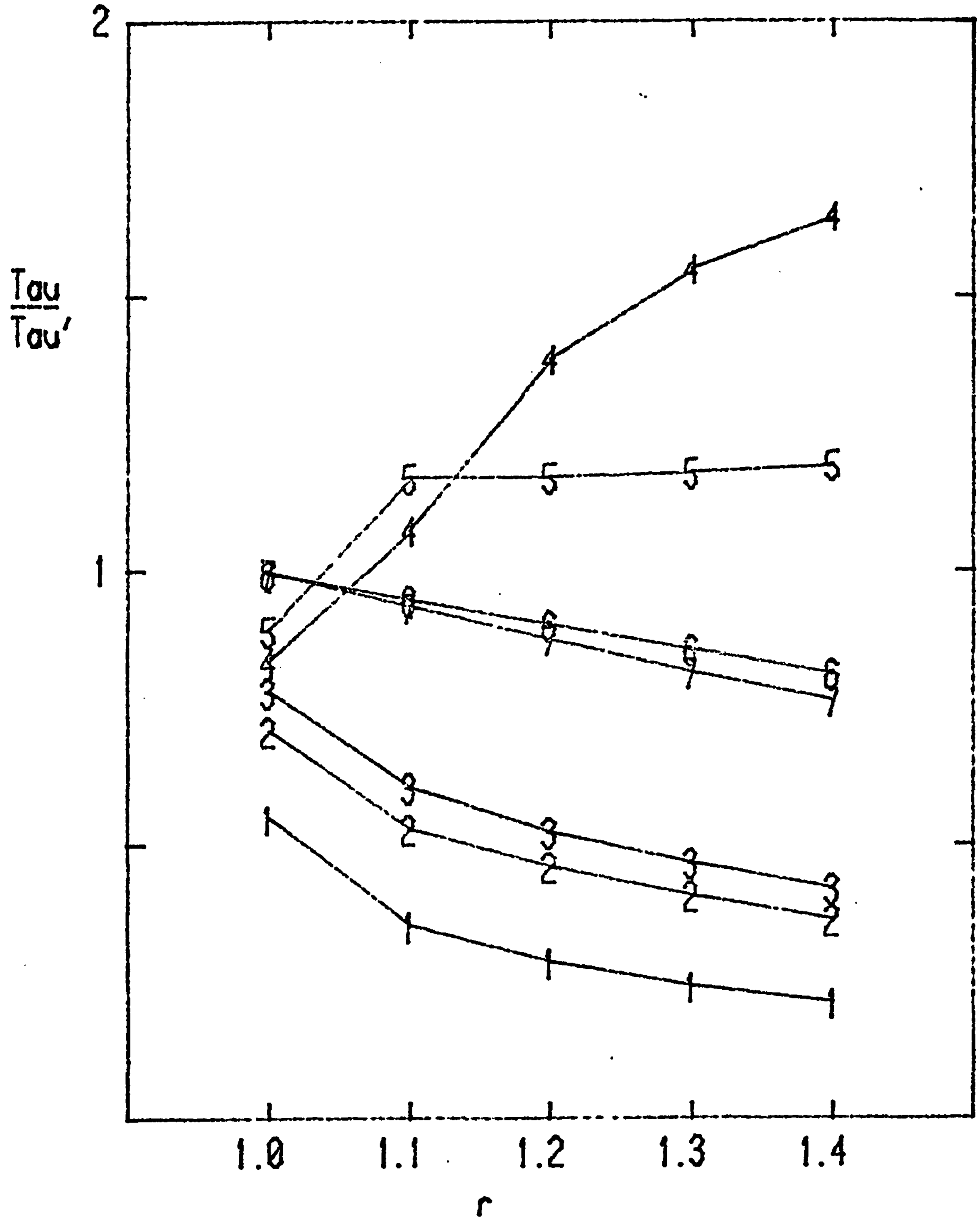

Figure 28. Si II λ6355, non-isothermal, solar

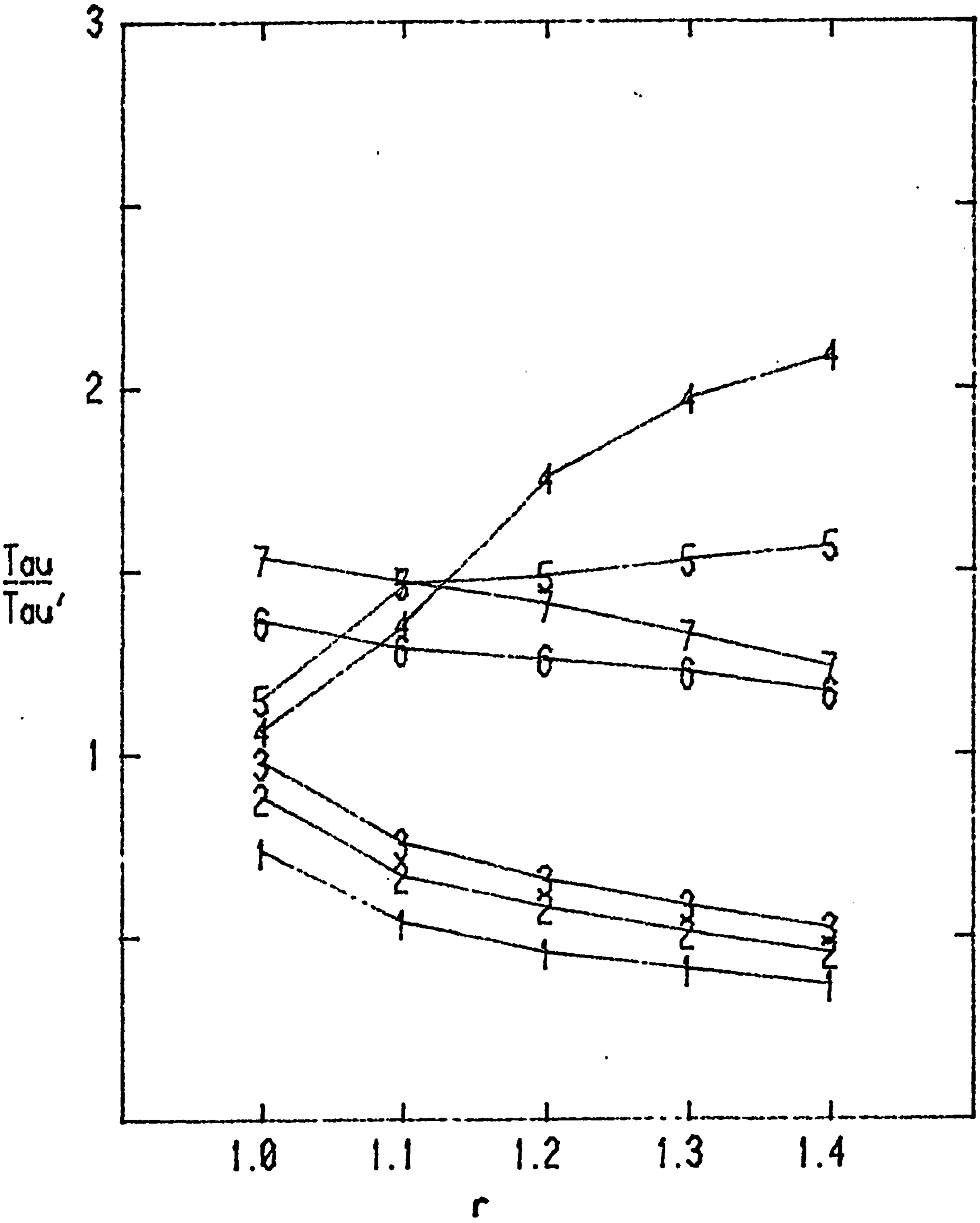

Figure 29. Si II λ4130, non-isothermal, solar

26 and 28, we see that at the earliest and latest times there is no effect for the λ6355 transition. At intermediate times, increasing the Si density increases the continuum optical depth from the ground, thus decreasing the ionization. This increases the density of Si II, as long as higher ionization stages dominate, increasing all line optical depths. For the case of no hydrogen shown in Figure 26, helium is the dominant electron source and it recombines by $t-t_0$ = 15 days. The resulting decrease in electron density causes Si III to be the dominant ion. For the other two compositions, the electron density remains larger and Si II and Si III have roughly equal densities. This explains the changing behavior of S/S' due to varying chemical composition at the time marked '5'. Comparison of Figures 16, 27 and 29 for the λ4130 transition show the same effects. Small differences are due to minor differences in the excitation of the lower levels for the λ4130 and λ6355 transitions.

Discontinuous Opacity Model

Numerical difficulties were encountered in solving the set of simultaneous equations for this model, so only a brief discussion will be given. Solutions were obtained for hydrogen in Type II envelopes for times up to 15 days past maximum light. The cutoff frequency, ν_c, could have reasonably been chosen anywhere between 7.5×10^{14} Hz and 1×10^{15} Hz, corresponding to 4000 Å and 3000 Å respectively. The Balmer continuum begins at $\nu = 8.2 \times 10^{14}$ Hz, so choosing $\nu_c = 8 \times 10^{14}$ Hz includes the Balmer and Lyman continuum and lines inside the photosphere while all other lines and continua are treated in the dilute case. This procedure was adopted.

The source function ratios for the first four Balmer lines are shown in Figures 30 through 33 using the same notation as previously for hydrogen. The line optical depth ratios for Hα are shown in Figure 34. The principal reason for the behavior of both the source function and the line optical depths is that the n=2 level is overpopulated with respect to all other level populations near those of LTE on the average since these lines are inside the photosphere. However, lines which have significant escape probabilities will tend to overpopulate the lower level of the transition as photons are lost. At the earliest times, the larger electron density causes larger collisional rates out of the upper levels, keeping the escape probability low for transitions among them and keeping their populations near those of LTE. However, the escape probabilities of lower levels are not as affected by collisions and are significant for Hα and Paschen α allowing an overpopulation of the n=2 and n=3 levels. As time increases, the expanding, cooling envelope causes the electron densities to drop, increasing the escape probabilities in transitions among the upper levels. This causes the upper levels to become more overpopulated and decreases the overpopulation of the lower levels since the Lyman lines still tend to enforce the average populations for $n \geq 2$ to be near LTE.

Accuracy

Now that we've seen the results, how accurate are they? As discussed earlier, radiative rates dominate in the lines of interest. Inspection of the rates in all other transitions shows that, with a few exceptions, radiative rates are always dominant. Therefore, the

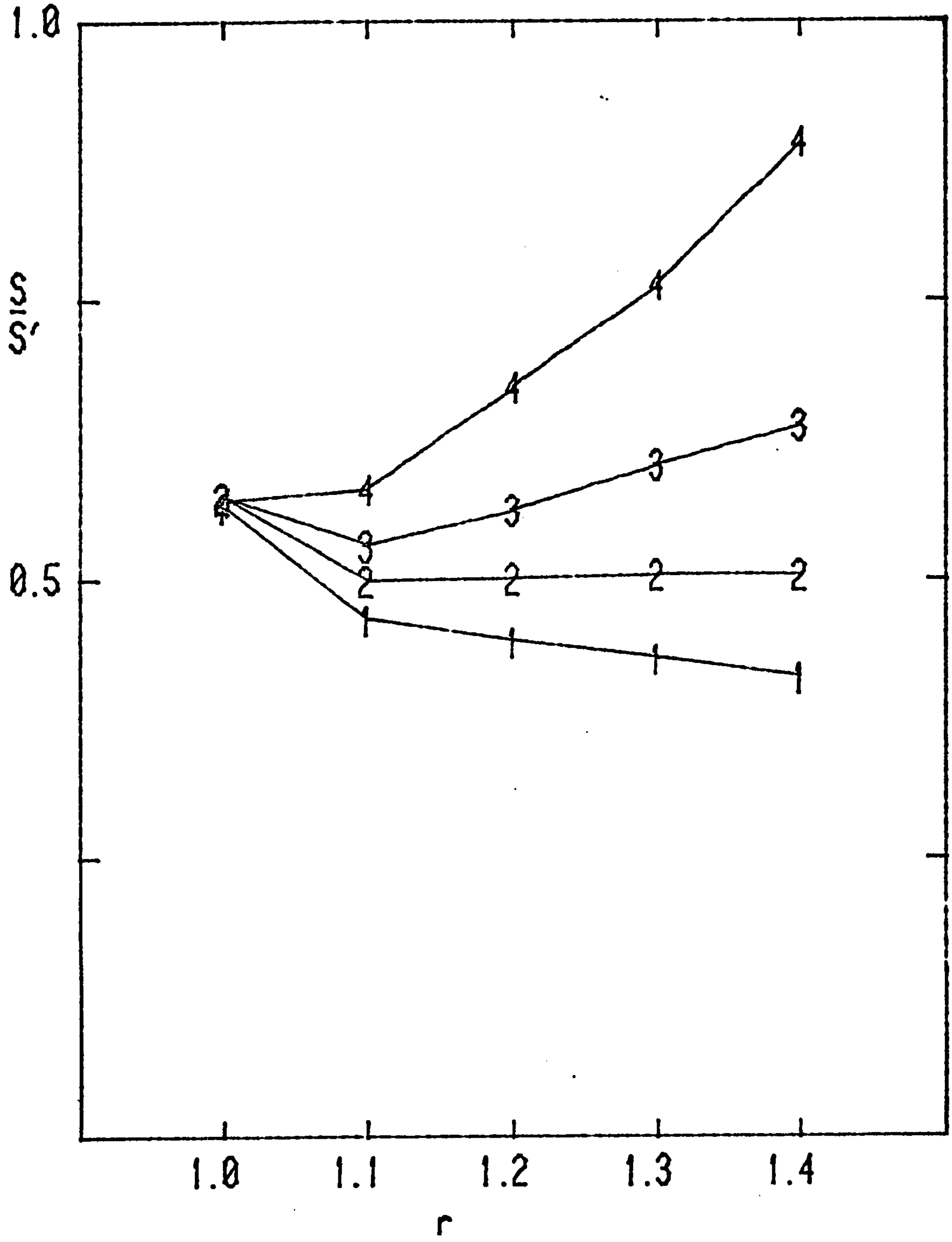

Figure 30. Hα, discontinuous opacity

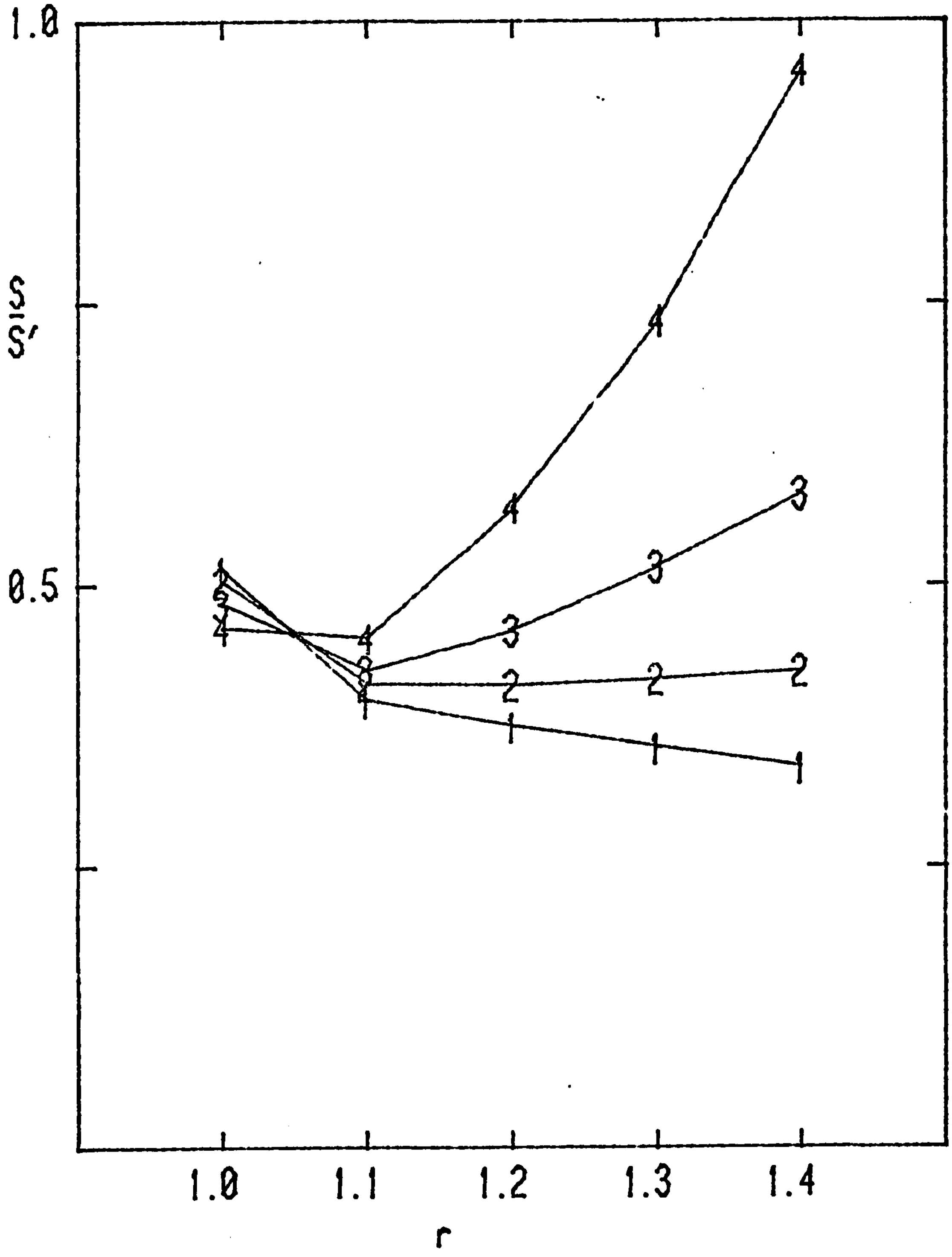

Figure 31. Hβ, discontinuous opacity

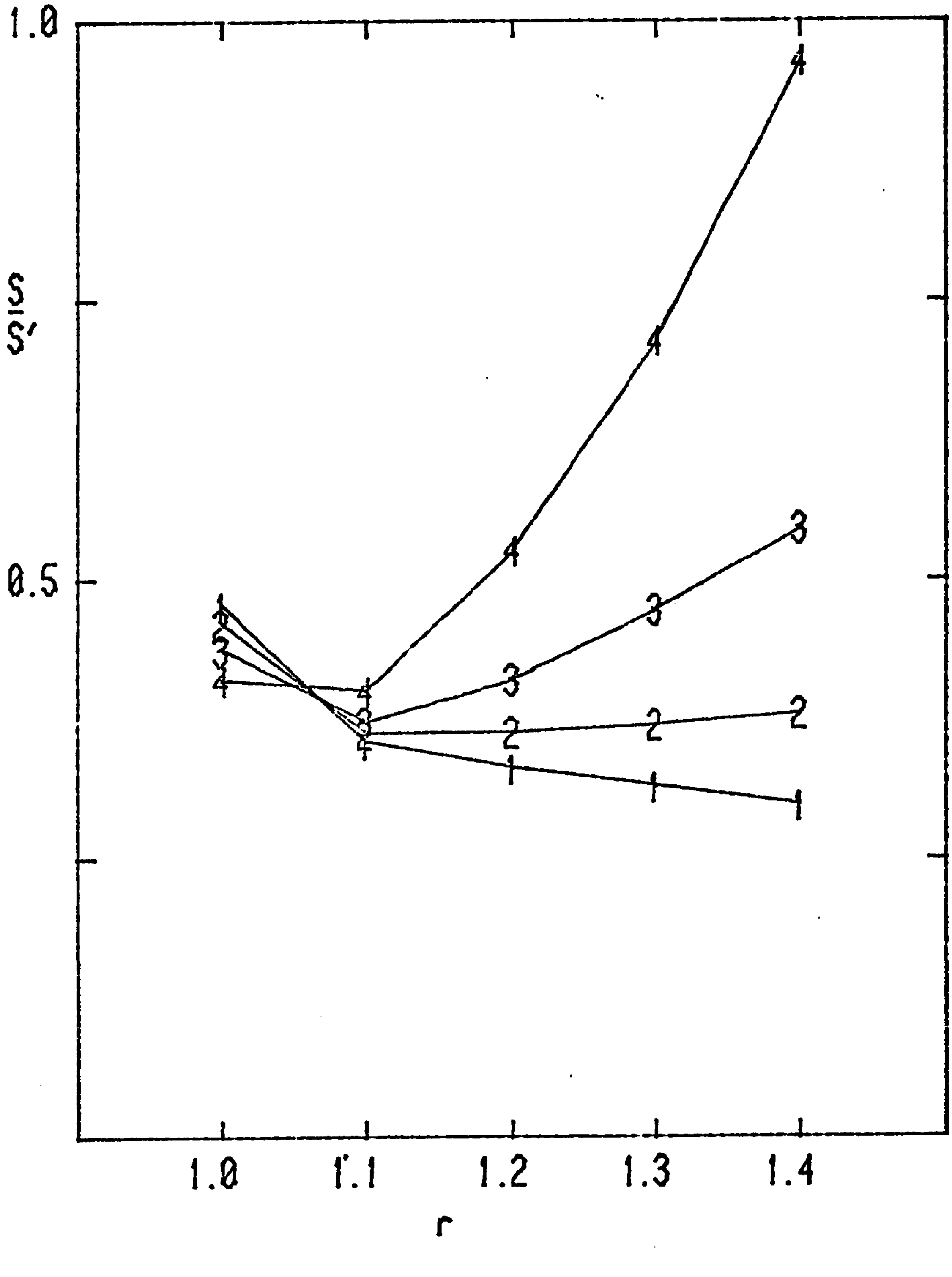

Figure 32. HY, discontinuous opacity

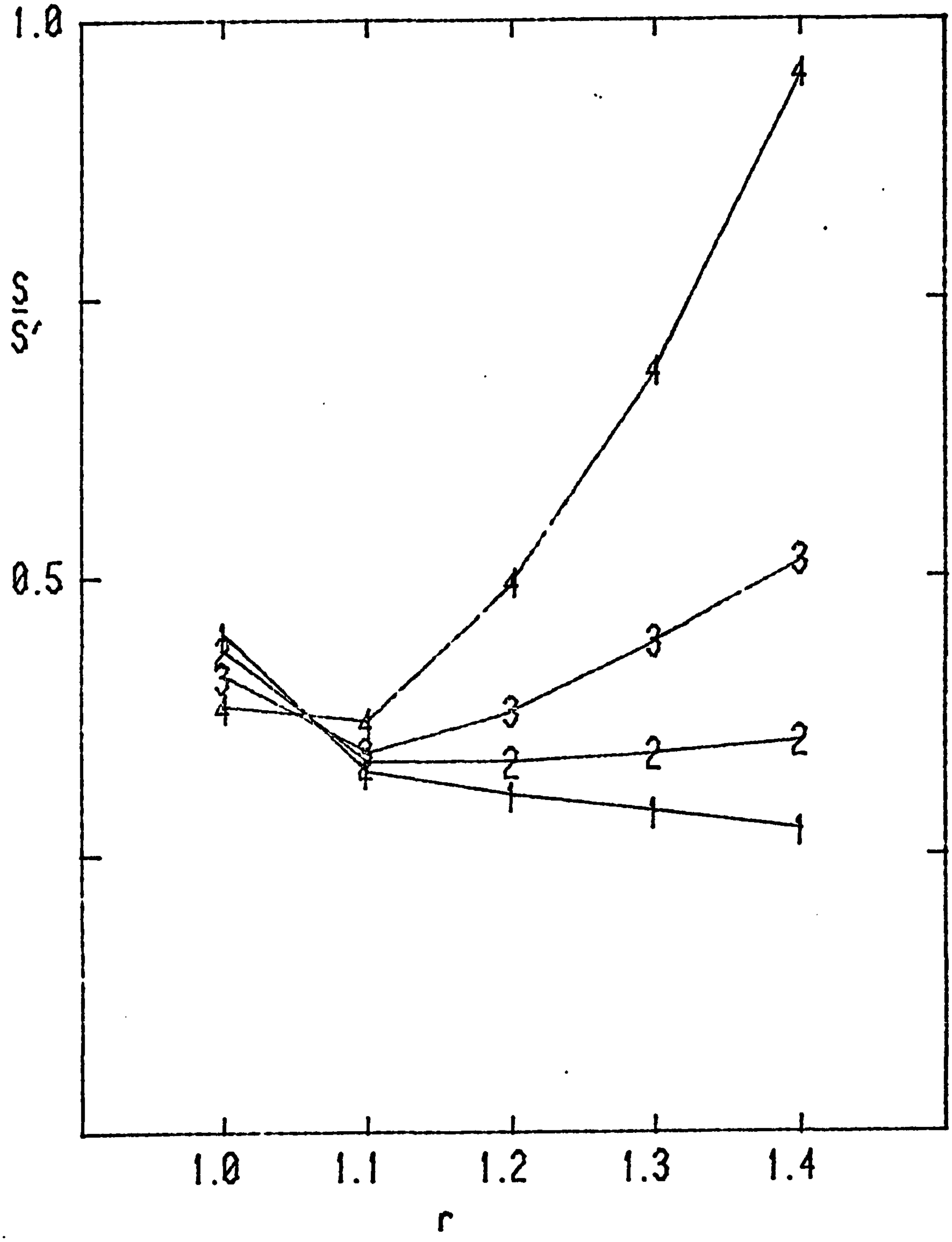

Figure 33. Hδ, discontinuous opacity

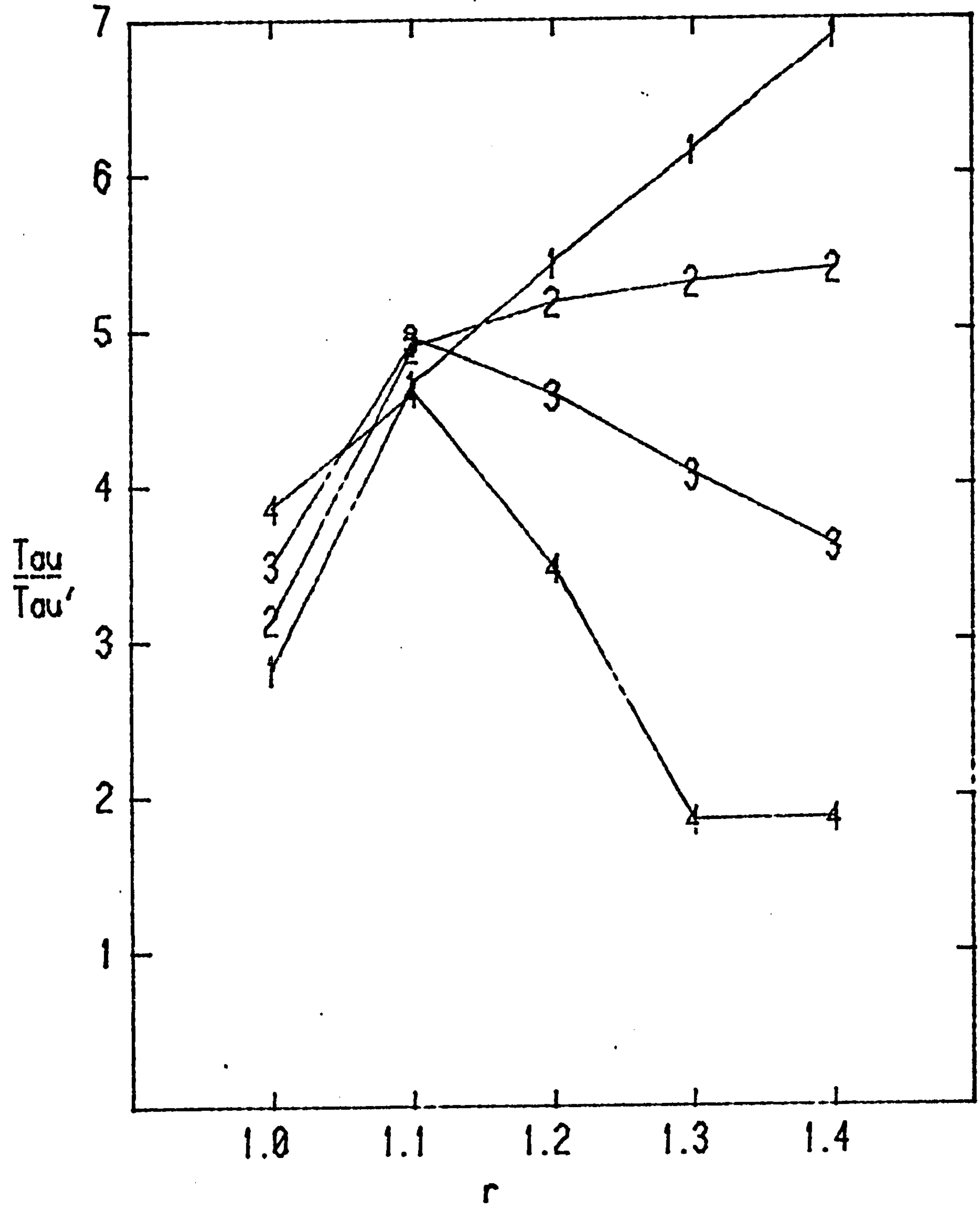

Figure 34. Hα, discontinuous opacity

accuracy of the results depend on the accuracy of three things: the oscillator strengths, the photoionization cross-sections and the convergence accuracy.

For hydrogen, the oscillator strengths should be accurate to within 1% [Wiese, et.al., 1969], and the photoionization cross-sections are accurate to 10% due to the Gaunt factors used [Allen, 1973]. The oscillator strengths for Si II are less accurately known. Those of the strongest transitions are probably accurate to 25% [Wiese, et.al, 1969], while for weaker transitions, errors by factors of five may not be unusual. It is difficult to assess the accuracy of the photoionization cross-sections for Si II. Since a cross-section of a few times 10^{-18} cm^2 is ordinary, order of magnitude errors are quite unlikely. On the average, these cross-sections are probably accurate within a factor of two or three.

The convergence accuracy was tested by applying a more stringent requirement than normal to sample cases. By requiring the change in all populations to be less than 0.001 rather than 0.01, the results were affected by less than 1%.

The overall accuracy of the results, then, is limited by the accuracy of the photoionization cross-sections. For hydrogen, the results should be accurate to within 10%, while for Si II any results which depend on the ionization may be off by fairly large factors. However, the similarities between the results for Si II and hydrogen suggest that the accuracy for Si II is within 50%.

Conclusions

The main question to be answered here was whether crude estimations could produce reasonably accurate level populations in supernova envelopes. Since the spectra are not well understood, certainly a factor of two is quite "reasonable accuracy." For the dilute models, all of the calculated source functions and line optical depths were, with a few exceptions, within a factor of two of those predicted. The discontinuous opacity model showed differences as large as factors of seven in the line optical depths. However, this model is an extreme which should place upper limits on the deviations which might be found from an opacity which increases uniformly with decreasing wavelength.

Therefore, certainly for predicting the absence or presence of lines, the crude predictions can be quite useful. Work done along these lines [Branch, private communication] has shown great promise, indicating that the dilute models predict most spectral features quite well with the exception of the Balmer lines in Type II supernovae. Since the calculated and predicted level populations for hydrogen are in rough agreement, this suggests that these lines are formed due to some physical aspect not considered in the models rather than a lack of understanding of the atomic processes involved.

Line profiles are more dependent on the variation of S and τ with radius, however. Future directions will include an investigation of the profiles produced by the accurate level populations.

REFERENCES

Allen, C.W. 1955, Astrophysical Quantities (London: Athlone Press).

Allen, C.W. 1973, Astrophysical Quantities (London: Athlone Press).

Arp, H.C. 1961, Ap. J., 133, 883.

Assousa, G.E., Peterson, C.J., Rubin, V.C., and Ford, W.K., Jr. 1976, Pub. A. S. P., 88, 828.

Baade, W. 1926, Astr. Nach., 228, 359.

Baade, W., and Zwicky, F. 1934, Proc. Nat. Acad. Sci. U.S., 20, 254.

Barbon, R., Ciatti, F., and Rosino, L. 1973, Astr. Ap., 25, 241.

Barbon, R., Ciatti, F., and Rosino, L. 1979, Astr. Ap., 72, 287.

Branch, D. 1977, M. N. R. A. S., 179, 401.

Branch, D. 1979, M. N. R. A. S., 186, 609.

Branch, D., and Bettis, C. 1978, A. J., 83, 224.

Branch, D., and Patchett, B. 1973, M. N. R. A. S., 161, 71.

Bychkova, V.S., and Bychkov, K.V. 1977, Soviet Astr. - A. J., 21, 435.

Castor, J.I. 1970, M. N. R. A. S., 149, 111.

Castor, J.I., and Nussbaumer, H. 1972, M. N. R. A. S., 155, 293.

Castor, J.I., and Van Blerkom, D. 1970, Ap. J., 161, 485.

Chevalier, R.A. 1976, Ap. J., 207, 872.

Chevalier, R.A. 1980, preprint.

Ciatti, F., and Rosino, L. 1977a, Astr. Ap., 56, 59.

Ciatti, F., and Rosino, L. 1977b, Astr. Ap., 57, 73.

Clark, D.H., and Stephenson, F.R. 1976, Q.J.R. Astr. Soc., 17, 290.

Colgate, S.A., and McKee, C. 1969, Ap. J., 157, 623.

Curtis, L.J., and Smith, W.H. 1974, Phys. Rev. A, 9, 1537.

REFERENCES (cont'd)

Falk, S.W., and Arnett, W.D. 1977, Ap. J. Suppl., 33, 515.

Feldt, A.N. 1979, Proc. Okla. Acad. Sci., 59, 94.

Gordon, C. 1975, Ap. J., 198, 765.

Griem, H.R. 1963, Phys. Rev., 131, 1170.

Holm, A.V., Wu, C.-C., and Caldwell, J.J. 1974, Pub. A. S. P., 86, 296.

Johnson, L.C. 1972, Ap. J., 174, 227.

Johnson, W.A. 1936, Harvard Bull. No. 902.

Karp, A.H. 1980, J. Q. S. R. T., in press.

Karp, A., Lasher, G., Chan, K.L., and Salpeter, E.E. 1977, Ap. J., 214, 161.

Kirshner, R.P., and Kwan, J. 1974, Ap. J., 193, 27.

Kirshner, R.P., Arp, H.C., and Dunlap, J.R. 1976, Ap. J., 207, 44.

Kurucz, R.L., and Peytremann, E. 1975, SAO Special Report No. 362.

Lasher, G. 1975, Ap. J., 201, 194.

Lasher, G., Karp, A.H., and Chan, K.L. 1977, in Supernovae, ed. D.N. Schramm (Dordrecht: Reidel), p.13.

Livingston, A.E., and Kernahan, J.A., Irwin, D.J.G., and Pinnington, E.H. 1976, J. Phys. B, 9, 389.

Mihalas, D. 1978, Stellar Atmospheres (San Francisco: W.H. Freeman and Company).

Minkowski, R. 1941, Pub. A. S. P., 53, 224.

Mustel', Eh.R. 1975, Soviet Astr. - A. J., 19, 685.

Oegerle, W.R., and Van Blerkom, D. 1976a, Ap. J., 206, 150.

Oegerle, W.R., and Van Blerkom, D. 1976b, Ap. J., 208, 453.

Oke, J.B., and Searle, L. 1974, Ann. Rev. Astr. Astrophys., 12, 315.

REFERENCES (cont'd)

Osterbrock, D.E. 1974, Astrophysics of Gaseous Nebulae (San Francisco: W.H. Freeman and Company).

Patchett, B., and Branch, D. 1972, M. N. R. A. S., 158, 375.

Patchett, B., and Wood, R. 1976, M. N. R. A. S., 175, 595.

Percival, I.C. 1966, Nuclear Fusion, 6, 182.

Pskovskii, Yu P. 1969, Soviet Astr. - A. J., 12, 750.

Ross, J.E., and Aller, L.H. 1976, Science, 191, 1223.

Schurmann, S.R., Arnett, W.D., and Falk, S.W. 1979, Ap. J., in press.

Seaton, M.J. 1964, Planet. Space Sci., 12, 55.

Sobolev, V.V. 1960, Moving Envelopes of Stars (Cambridge: Harvard University Press).

Tinsley, B.M. 1977a, in Supernovae, ed. D.N. Schramm (Dordrecht: Reidel), p.13.

Tinsley, B.M. 1977b, Ap. J., 216, 548.

Van Blerkom, D. 1973, in IAU Symposium 49, Wolf-Rayet and High-Temperature Stars, ed. M.K.V. Bappu and J.D. Sahade (Dordrecht: Reidel), p.165.

Van Blerkom, D. 1978, Ap. J., 221, 186.

Van Regemorter, H. 1962, Ap. J., 136, 906.

Wagoner, R.V. 1977, Ap. J. Lett., 214, L5.

Weaver, T.A., and Woosley, S.E. 1978, preprint.

Wiese, W.L., Smith, W.H., and Miles, B.M. 1969, Atomic Transition Probabilities, Vol. II NRDS-NBS 22, U.S. Govt. Printing Office.

Zwicky, F. 1965, in Stellar Structure, ed. L.H. Aller and D.B. McLaughlin (Chicago: The University of Chicago Press), p. 367.